Table 1 The sequences of siRNAs

	Sense strand	Antisense strand
PSMA7		
#1	5′-GAAGUAUGUUGCUGAAAUUUU-3′	5′-AAUUUCAGCAACAUACUUCUU-3′
#2	5′-GAAGAGACAUUGUUGUUCUUU-3′	5′-AGAACAACAAUGUCUCUUCUU-3′
#3	5′-GAAGAUCUGUGCUUUGGAUUU-3′	5′-AUCCAAAGCACAGAUCUUCUU-3′
#4	5′-CAUCGUGGGUUUCGACUUUUU-3′	5′-AAAGUCGAAACCCACGAUGUU-3′
RAN		
#1	5′-AGAAGAAUCUUCAGUACUAUU-3′	5′-UAGUACUGAAGAUUCUUCUUU-3′
#2	5′-GUGAAUUUGAGAAGAAGUAUU-3′	5′-UACUUCUUCUCAAAUUCACUU-3′
#3	5′-CCUAUUAAGUUCAAUGUAUUU-3′	5′-AUACAUUGAACUUAAUAGGUU-3′
#4	5′-ACAGGAAAGUGAAGGCGAAUU-3′	5′-UUCGCCUUCACUUUCCUGUUU-3′

Abbreviation: siRNA, small interfering RNAs.

added (4% paraformaldehyde, 0.1% Triton X-100, 1 μg/mL Hoechst 33342 in PBS). Twenty minutes after incubation, cells were washed with PBS. We determined the number of apoptotic cells was in three microscopic fields of each well by fluorescence microscopy.

Transfection of siRNA

We carried out transfection of HT-29 cells with siRNA using Liopfectamine 2000 (Invitrogen), according to the manufacturer's protocol. We plated HT-29 cells 24 hours before transfection, and we then transfected the cells, which were grown to 50% confluence, with 40 nM siRNAs.

Real-time RT-PCR

We purified total RNA from cells and tumor tissues with an RNeasy Mini Kit and RNase-Free DNase Set (QIAGEN, Hilden, Germany), and produced cDNAs with an ExScript RT reagent Kit (Takara Bio, Shiga, Japan). We then subjected cDNA samples to real-time PCR using SYBR Premix Ex Taq (Takara) and specific primers as follows: for *PSMA7*, forward, 5′-CAAGTGGAGTACGCGCAGGA-3′; reverse, 5′-CTGCAGTTTGGCCACTGACTTC-3′; for *RAN*, forward, 5′-AAGTTGTCATGGACCCAGCTTTG-3′; reverse, 5′-GCTGGGCTCCAGCTTCATTC-3′. We carried out the reactions using the 7300 Real-Time PCR System (Applied Biosystems, Foster City, CA, USA). We normalized gene-expression levels by 18S rRNA or *GAPDH*.

Cell-direct real-time RT-PCR

We used FastLane Cell cDNA Kit and QuantiTect SYBR Green PCR Kit (QIAGEN). We lysed cells in a well of cell transfection array and synthesized the first-strand cDNA. The cDNA template was then directly subjected to real-time RT-PCR using specific primers.

siRNA treatment *in vivo*

We performed animal experiments in compliance with the guidelines of the Institute for Laboratory Animal Research, National Cancer Center Research Institute of Japan. We subcutaneously injected 5×10^6 HT-29 cells into athymic nude mice (six-week-old females; CLEA Japan, Tokyo, Japan). When the HT-29 tumor grew to approximately 5–6 mm in diameter, we injected mice with 1 nmol siRNA by intratumoral injection. We harvested tumor tissues for analysis of mRNA and apoptosis at 24 and 72 hours after treatment, respectively.

TUNEL technique

We harvested tumor tissues 72 hours after administration of siRNA and prepared frozen sections. We then performed TUNEL (TdT-mediated dUTP nick-end labeling) staining using an *In Situ* Cell Death Detection Kit, Fluorescein (Roche Diagnostics, Basel, Switzerland), according to the manufacturer's protocol. DNA strand breaks in apoptotic cells can be labeled by the addition of fluorescein dUTP using terminal deoxynucleotidyl transferase (TdT). The nuclei were stained with DAPI. We determined the number of fluorescein-positive cells in three microscopic fields of each section by fluorescence microscopy.

Human samples

The study protocol for clinical samples was approved by the Institutional Review Board of Osaka University Medical School (Osaka, Japan), and written informed consent was

obtained from each patient. We obtained total RNA from tumor tissues and normal adjacent tissues (FirstChoice Human Tumor/Normal Adjacent Tissue RNA) from Ambion (Austin, TX, USA).

cDNA micro-array analysis

We performed cDNA micro-array analysis using AceGene (DNA Chip Research Inc., Yokohama, Japan) according to the manufacturer's instructions (http://www.dna-chip.co.jp/thesis/AceGeneProtocol.pdf) to obtain an expression profile of human colorectal cancer.[21] As a standard normal control reference, a mixture of total RNA extracted from normal colorectal tissues was used. We synthesized cDNA from total RNA of normal colorectal tissues and colorectal tumor tissues, and labeled cDNA with Cy3 for normal colorectal tissue, and Cy5 for colorectal tumor tissues, respectively. After hybridization of cDNA and array, the array was scanned, and Cy5/Cy3 ratios were $\log_2$-transformed to compare levels of mRNA expression in tumor and normal tissues.

Statistical analysis

We conducted statistical analysis using the analysis of variance with Student's *t*-test. We considered a *P* value of 0.05 or less as a significant difference.

Results

RNAi-based screening for identification of molecular targets

To identify molecular targets for therapy, we conducted a study of RNAi-induced gene knockdown in HT-29 human colon cancer cells. The strategy for target identification is schematically shown in Figure 1. We performed gene expression profiling of 191 subjects with colorectal tumors and selected 97 genes whose expression was elevated in human colorectal cancer tissues by rank order of mRNA expression (Table 2). We used the siRNAs specific to these genes which are siRNA pools composed of four distinct siRNA species targeting different sequences of the same target transcript for RNAi-based screening. We transfected HT-29 cells with the

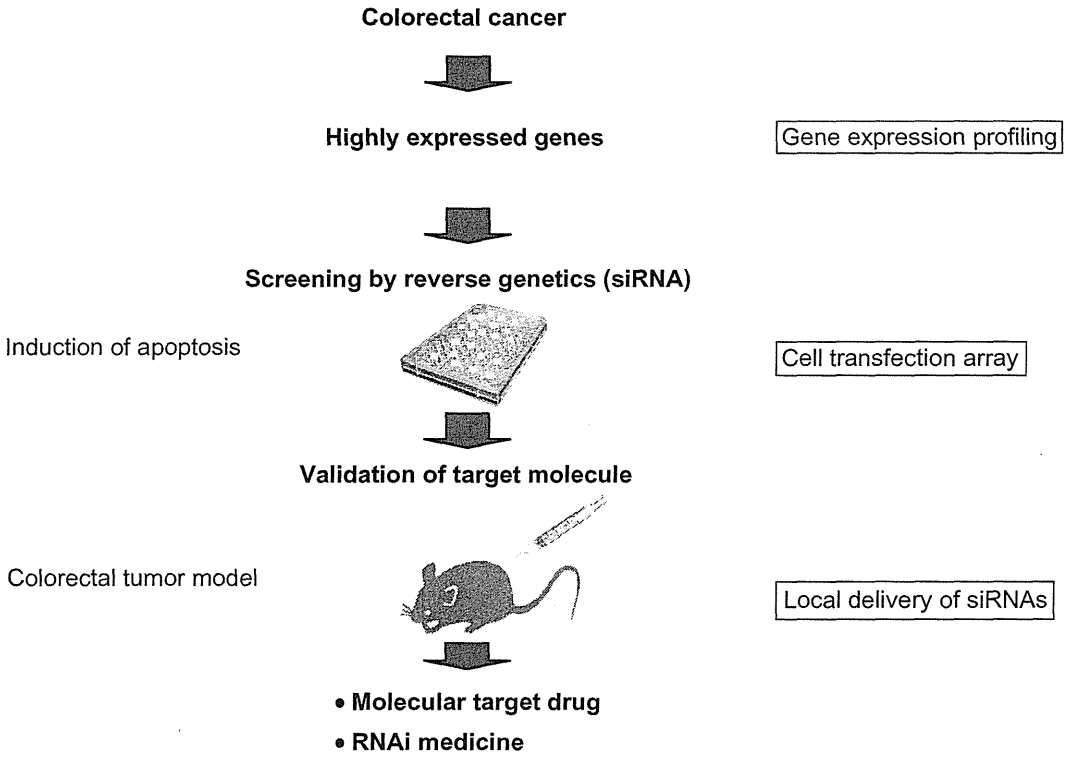

Figure 1 Schematic representation of the strategy for targets identification by RNAi-based reverse genetics *in vitro* and *in vivo*. First, we carried out a gene expression profiling of human colorectal tumor tissues and selected genes whose expression was elevated. We performed a functional screening of genes by a cell transfection array to test the efficacy of a specific siRNA related to apoptosis induction in human colorectal cancer. Subsequently, the siRNAs against candidate genes were applied to an *in vivo* animal tumor model. Finally, we identified new molecular targets for drug and RNAi-based colorectal cancer therapy.
Abbreviation: siRNA, small interfering RNAs.

Table 2 The list of 97 genes elevated in human colorectal tumor tissues

No	Gene	Description	Accession no.	Log_2 ratio (tumor/normal)
1	*COL1A1*	Collagen, type I, α1	NM_000088	2.137
2	*SPP1*	Secreted phosphoprotein 1 (osteopontin, bone sialoprotein I, early T-lymphocyte activation 1)	NM_000582	1.531
3	*CCL20*	Chemokine (C-C motif) ligand 20	NM_004591	1.501
4	*UBD*	Ubiquitin D	NM_006398	1.392
5	*TGFBI*	Transforming growth factor, β-induced, 68 kDa	NM_000358	1.345
6	*IFITM1*	Interferon induced transmembrane protein 1 (9–27)	NM_003641	1.341
7	*MMP12*	Matrix metallopeptidase 12 (macrophage elastase)	NM_002426	1.248
8	*CEACAM6*	Carcinoembryonic antigen-related cell adhesion molecule 6 (non-specific cross reacting antigen)	NM_002483	1.237
9	*RPS21*	Ribosomal protein S21	NM_001024	1.232
10	*PFDN4*	Prefoldin 4	NM_002623	1.209
11	*TIMP1*	TIMP metallopeptidase inhibitor 1	NM_003254	1.191
12	*NEK6*	NIMA (never in mitosis gene a)-related kinase 6	NM_014397	1.089
13	*MMP1*	Matrix metallopeptidase 1 (interstitial collagenase)	NM_002421	1.079
14	*S100A11*	S100 calcium binding protein A11 (calgizzarin)	NM_005620	1.055
15	*IFNAR1*	Interferon (α, β and ω) receptor 1	NM_000629	1.031
16	*CPSF4*	Cleavage and polyadenylation specific factor 4, 30 kDa	NM_006693	1.024
17	*TMEPAI*	Transmembrane, prostate androgen induced RNA	NM_020182	1.013
18	*RPL31*	Ribosomal protein L31	NM_000993	0.995
19	*CPNE3*	Copine III	NM_003909	0.988
20	*UBE2C*	Ubiquitin-conjugating enzyme E2C	NM_007019	0.979
21	*NQO1*	NAD(P)H dehydrogenase, quinone 1	NM_000903	0.968
22	*MYC*	V-myc myelocytomatosis viral oncogene homolog (avian)	NM_002467	0.966
23	*LCN2*	Lipocalin 2 (oncogene 24p3)	NM_005564	0.959
24	*PRKAA1*	Protein kinase, AMP-activated, α1 catalytic subunit	NM_006251	0.958
25	*GNGT2*	Guanine nucleotide binding protein (G protein), gamma transducing activity polypeptide 2	NM_031498	0.932
26	*PSMA7*	Proteasome (prosome, macropain) subunit, α-type, 7	NM_002792	0.932
27	*SLC3A2*	Solute carrier family 3 (activators of dibasic and neutral amino acid transport), member 2	NM_002394	0.925
28	*C10ORF137*	Chromosome 10 open reading frame 137	NM_015608	0.917
29	*CKS2*	CDC28 protein kinase regulatory subunit 2	NM_001827	0.912
30	*RPS6*	Ribosomal protein S6	NM_001010	0.911
31	*RPL39*	Ribosomal protein L39	NM_001000	0.910
32	*COL10A1*	Collagen, type X, α1(Schmid metaphyseal chondrodysplasia)	NM_000493	0.910
33	*MLLT1*	Myeloid/lymphoid or mixed-lineage leukemia (trithorax homolog, Drosophila); translocated to, 1	NM_005934	0.896
34	*GABRD*	γ-aminobutyric acid (GABA) A receptor, δ	NM_000815	0.895
35	*COL1A2*	Collagen, type I, α2	NM_000089	0.894
36	*DKFZP564O0463*	WD repeats and SOF1 domain containing	NM_015420	0.894
37	*RIPK2*	Receptor-interacting serine-threonine kinase 2	NM_003821	0.893

(*Continued*)

Table 2 *(Continued)*

No	Gene	Description	Accession no.	Log_2 ratio (tumor/normal)
38	*FOXM1*	Forkhead box M1	NM_021953	0.892
39	*PIGL*	Phosphatidylinositol glycan, class L	NM_004278	0.870
40	*NIN*	Ninein (GSK3B interacting protein)	NM_016350	0.870
41	*ATP2B1*	ATPase, Ca^+ transporting, plasma membrane 1	NM_001682	0.870
42	*MIF*	Macrophage migration inhibitory factor (glycosylation-inhibiting factor)	NM_002415	0.861
43	*PCYOX1*	Prenylcysteine oxidase 1	NM_016297	0.850
44	*ARF4*	ADP-ribosylation factor 4	NM_001660	0.843
45	*MEOX2*	Mesenchyme homeo box 2 (growth arrest-specific homeo box)	NM_005924	0.840
46	*HTR2B*	5-hydroxytryptamine (serotonin) receptor 2B	NM_000867	0.836
47	*HRASLS3*	HRAS-like suppressor 3	NM_007069	0.827
48	*GYPA*	Glycophorin A (includes Ss blood group)	NM_002099	0.819
49	*GDF15*	Growth differentiation factor 15	NM_004864	0.817
50	*NPHS2*	Nephrosis 2, idiopathic, steroid-resistant (podocin)	NM_014625	0.816
51	*FIBL-6*	Hemicentin 1	NM_031935	0.804
52	*AKAP8L*	A kinase (PRKA) anchor protein 8-like	NM_014371	0.787
53	*SLC12A2*	Solute carrier family 12 (sodium/potassium/ chloride transporters), member 2	NM_001046	0.784
54	*CDK10*	Cyclin-dependent kinase (CDC2-like) 10	NM_003674	0.781
55	*UFM1*	Ubiquitin-fold modifier 1	NM_016617	0.780
56	*TBX19*	T-box 19	NM_005149	0.775
57	*DPEP1*	Dipeptidase 1 (renal)	NM_004413	0.775
58	*NNMT*	Nicotinamide N-methyltransferase	NM_006169	0.754
59	*RPS20*	Ribosomal protein S20	NM_001023	0.748
60	*ZNF84*	Zinc finger protein 84 (hpf2); znf84	NM_003428	0.740
61	*HIG2*	Hypoxia-inducible protein 2	NM_013332	0.639
62	*SNAI2*	Snail homolog 2 (Drosophila)	NM_003068	0.610
63	*SLAMF7*	SLAM family member 7	NM_021181	0.604
64	*RAN*	RAN, member RAS oncogene family	NM_006325	0.603
65	*SNAI1*	Snail homolog 1 (Drosophila)	NM_005985	0.580
66	*MRAS*	Muscle RAS oncogene homolog	NM_012219	0.543
67	*ARHGEF4*	Rho guanine nucleotide exchange factor (GEF) 4	NM_015320	0.536
68	*MDK*	midkine (neurite growth-promoting factor 2)	NM_002391	0.530
69	*BRAF*	Y-raf murine sarcoma viral oncogene homolog B1	NM_004333	0.528
70	*FBXO11*	F-box protein 11	NM_012167	0.519
71	*AATF*	Apoptosis antagonizing transcription factor	NM_012138	0.516
72	*FIGN*	Fidgetin	NM_018086	0.506
73	*MMP9*	Matrix metallopeptidase 9 (gelatinase B, 92kDa gelatinase, 92kDa type IV collagenase)	NM_004994	0.497
74	*VEGFA*	Vascular endothelial growth factor	NM_003376	0.496
75	*FBXW5*	F-box and WD-40 domain protein 5	NM_178225	0.481
76	*LTA*	Lymphotoxin α (TNF superfamily, member 1)	NM_000595	0.476
77	*TRAP1*	TNF receptor-associated protein 1	NM_016292	0.455
78	*LGALS1*	Lectin, galactoside-binding, soluble, 1 (galectin 1)	NM_002305	0.453
79	*RRAS*	Related RAS viral (r-ras) oncogene homolog	NM_006270	0.441
80	*MMP10*	Matrix metallopeptidase 10 (stromelysin 2)	NM_002425	0.440

(Continued)

Table 2 (*Continued*)

No	Gene	Description	Accession no.	Log_2 ratio (tumor/normal)
81	*FBXW11*	F-box and WD-40 domain protein 11	NM_012300	0.440
82	*SAT*	Spermidine/spermine N1-acetyltransferase	NM_002970	0.440
83	*RPN2*	Ribophorin II	NM_002951	0.400
84	*RAB4B*	RAB4B, member RAS oncogene family	NM_016154	0.398
85	*FETUB*	Fetuin B	NM_014375	0.395
86	*ELF4*	E74-like factor 4 (ets domain transcription factor)	NM_001421	0.388
87	*SHAX3*	Chromatin modifying protein 4C	NM_152284	0.387
88	*ECT2*	Epithelial cell transforming sequence 2 oncogene	NM_018098	0.384
89	*HES6*	Hairy and enhancer of split 6 (Drosophila)	NM_018645	0.383
90	*DDEF1*	Development and differentiation enhancing factor 1	NM_018482	0.378
91	*RHEB*	Ras homolog enriched in brain	NM_005614	0.375
92	*CTNND1*	Catenin (cadherin-associated protein), δ1	NM_001331	0.368
93	*DNMT3B*	DNA (cytosine-5-)-methyltransferase 3β	NM_006892	0.365
94	*ASPM*	ASP (abnormal spindle)-like, microcephaly associated (Drosophila)	NM_018136	0.360
95	*PCDHA10*	Protocadherin α10	NM_018901	0.349
96	*VEGFC*	Vascular endothelial growth factor C	NM_005429	0.347
97	*RASGRF1*	Ras protein-specific guanine nucleotide-releasing factor 1	NM_002891	0.346

siRNAs using reverse transfection-based cell transfection array. To evaluate the efficiency of the cell transfection array, we used GAPDH siRNA against the gene encoding GAPDH (glyceraldehyde-3-phosphate dehydrogenase). GAPDH siRNA transfer caused an approximate 75% reduction of the GAPDH mRNA expression in HT-29 cells relative to the control nontargeting siRNA (data not shown).

We assessed siRNAs for their ability to induce apoptosis in HT-29 compared with the control nontargeting siRNA. We measured cell viability by resazurin reduction and examined apoptosis by caspase-3/7 activity. Caspase-3/7 activity was normalized by viable cell number (measurement value of resazurin reduction) and Caspase-3/7 activation by siRNAs was compared with control nontargeting siRNA. The results indicated that the downregulation of 11 genes (*TIMP1*, *S100A11*, *TMEPAI*, *PSMA7*, *COL10A1*, *RAN*, *VEGFA*, *LTA*, *TRAP1*, *MMP10*, and *RHEB*) resulted in a marked induction of apoptosis in HT-29 cells (caspase-3/7 activity, percentage of nontargeting siRNA > 200, $P < 0.05$, Figure 2). In particular, the PSMA7 siRNA pool and the RAN siRNA pool strongly enhanced caspase-3/7 activity (caspase-3/7 activity, percentage of nontargeting siRNA > 300, $P < 0.001$, Figure 2). We validated these results by counting Hoechst-stained cells showing apoptotic nuclear condensation and fragmentation (Figure 3A) and found that there was a significantly higher apoptotic cell death rate in cells given PSMA7 siRNA pool and RAN siRNA pool relative to that in cells given control siRNA ($P < 0.01$, Figure 3B). At 72 hours after treatment with siRNA, there was substantial cell death induced by the PSMA7 siRNA pool and the RAN siRNA pool compared with the control nontargeting siRNA (Figure 3C).

We assessed the efficacy of PSMA7 siRNA pool and RAN siRNA pool for the knockdown of mRNA by cell-direct real-time RT-PCR analysis. This analysis revealed that PSMA7 siRNA pool and RAN siRNA pool inhibited the mRNA expression relative to the control nontargeting siRNA, 80% and 60% respectively (Figure 3D). To evaluate the knockdown efficiency of individual siRNAs of the siRNA pool, we performed a liposome-mediated siRNA transfection. PSMA7 siRNA #2 and RAN siRNA #4 most efficiently silenced PSMA expression (70% reduction of mRNA) and RAN expression (70% reduction of mRNA), respectively (Figure 3E). We also confirmed that PSMA7 siRNA #2 and RAN siRNA #4 strongly increased caspase-3/7 activity in HT-29 cells (data not shown). PSMA7 siRNA #2 and RAN siRNA #4 were used in further *in vivo* experiments.

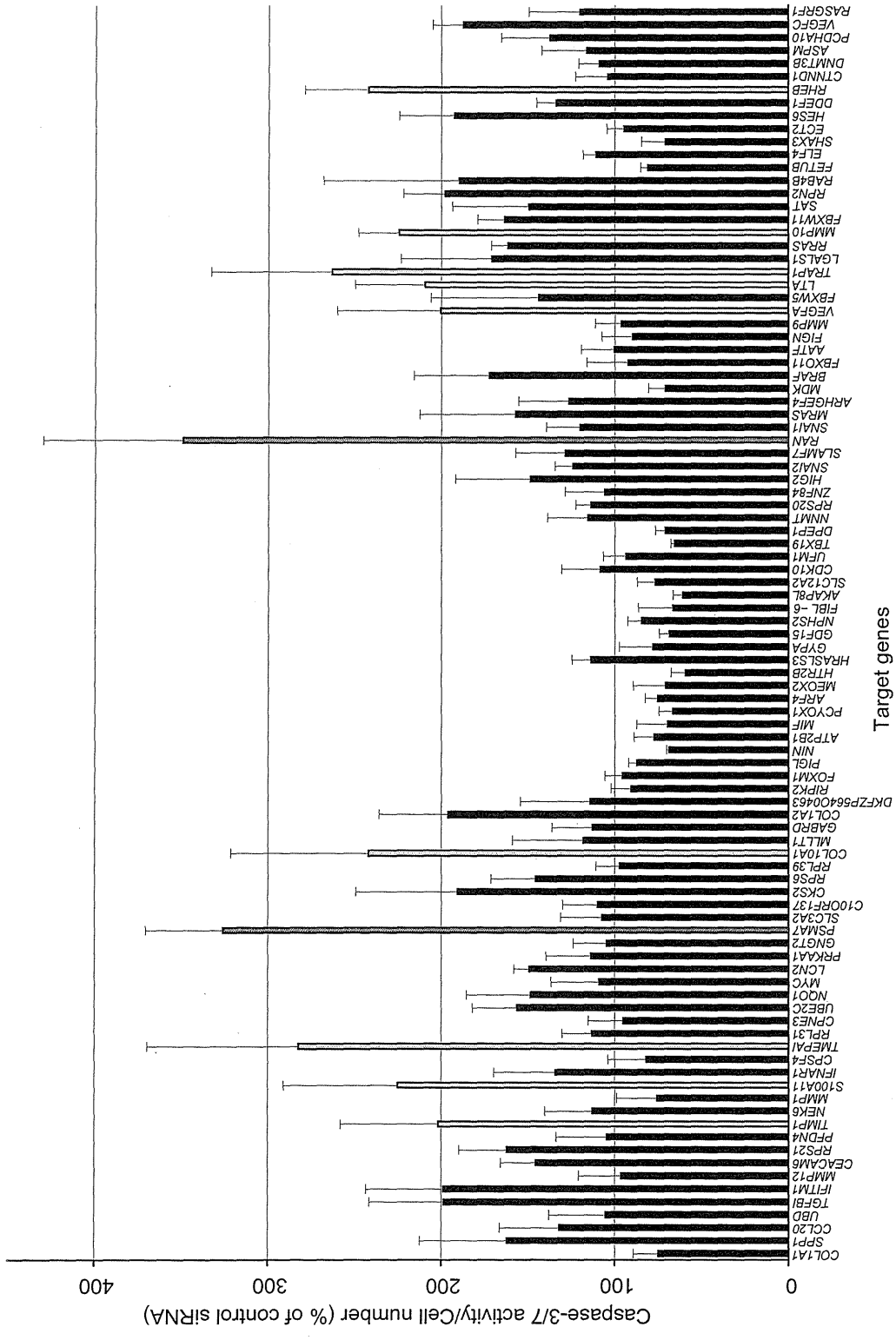

Figure 2 Functional screening of genes by RNAi-cell transfection array in cultured colorectal cancer cells. Cell number and caspase-3/7 activity were measured 72 hours after transfection of HT-29 cells. Caspase-3/7 activity was normalized by viable cell number to evaluate apoptosis induction. Control nontargeting siRNA is set to 100% and relative activity is shown. Yellow color bar: relative activity (%) >200, $P < 0.05$; blue color bar: relative activity (%) >300, $P < 0.001$. n = 4 per group. Values are mean ± SD.
Abbreviations: SD, standard deviation; siRNA, small interfering RNAs.

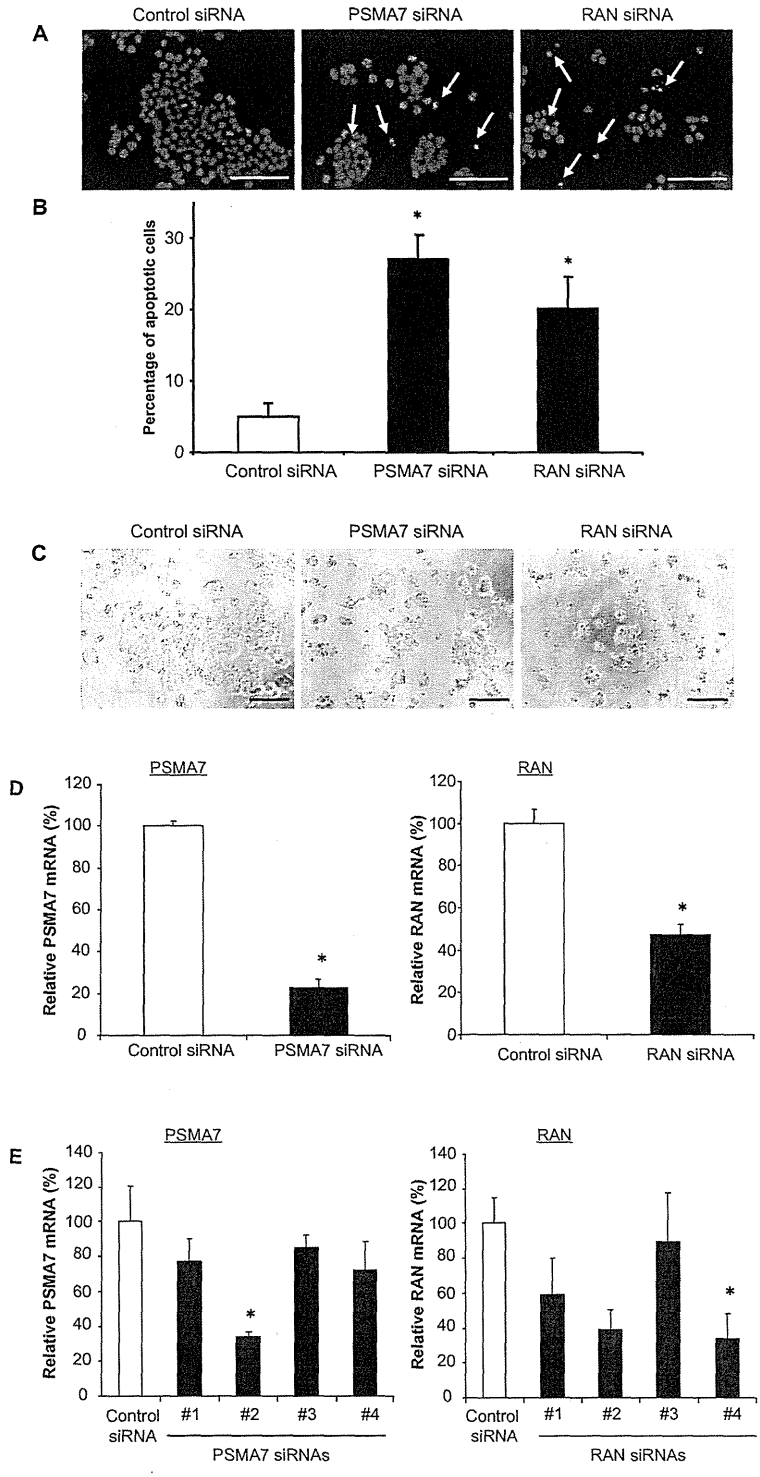

Figure 3 Apoptosis of HT-29 cells transduced with PSMA7 siRNA and RAN siRNA. **A)** Hoechst staining of cells 72 hours after the transfection of siRNA. Scale bar, 100 μm. The arrows indicate cells with nuclear condensation and fragmentation. **B)** Numbers of apoptotic cells from (A). The data show the percentage of apoptotic cells. As a control, nontargeting control siRNA was used ($n = 4$ per group, $^*P < 0.01$). **C)** Phase contrast micrograph of HT-29 cells 72 hours after the treatment of siRNA. Scale bar, 200 μm. **D)** Knockdown of mRNA by PSMA7 siRNA pool and RAN siRNA pool using cell transfection array was measured 72 hours after transfection. ($n = 5$ per group, $^*P < 0.001$). **E)** Knockdown of mRNA by PSMA7 siRNAs and RAN siRNAs. Expression of PSMA7 mRNA and RAN mRNA was measured 72 hours and 48 hours after transfection, respectively ($n = 3$ per group, $^*P < 0.01$). As a control, nontargeting siRNA was used. Values are mean ± SD.

Abbreviations: PSMA7, proteasome subunit, α-type, 7; RAN, ras-related nuclear protein; SD, standard deviation; siRNA, small interfering RNAs.

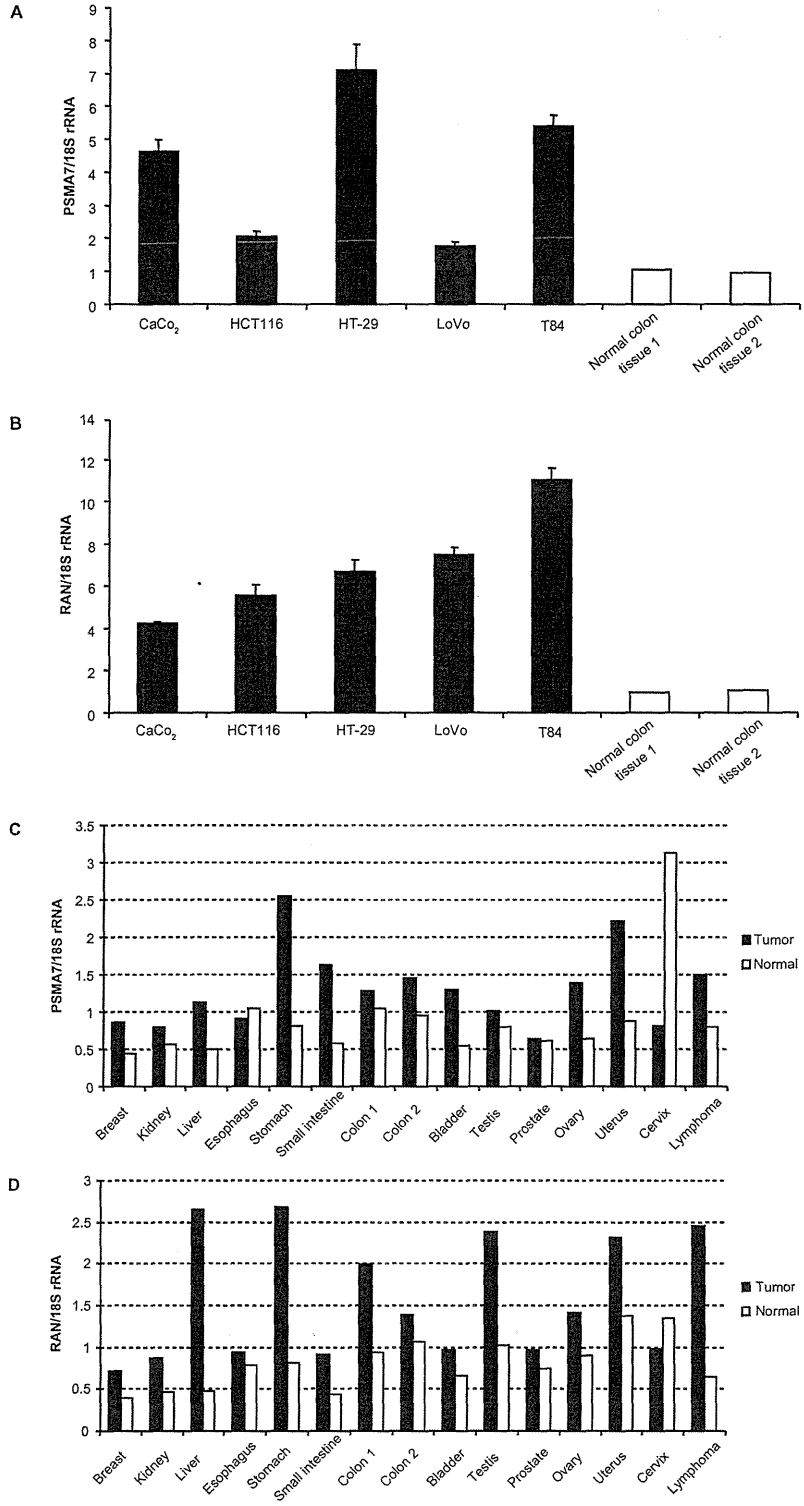

Figure 4 *PSMA7* and *RAN* expression in colorectal cancer cell lines and tumor tissues. PSMA7 mRNA and RAN mRNA expression were analyzed by real-time RT-PCR. **A**) PSMA7 mRNA expression in colorectal cancer cell lines. $n = 3$ per group. Values are mean ± SD. **B**) RAN mRNA expression in colorectal cancer cell lines. $n = 3$ per group. Values are mean ± SD. **C**) PSMA7 mRNA expression in various tumor tissues (■, $n = 1$) and their normal adjacent tissues (□, $n = 1$). **D**) RAN mRNA expression in various tumor tissues (■, $n = 1$) and their normal adjacent tissues (□, $n = 1$). mRNA expression was normalized to 18S rRNA. Mean of normal colon tissues is set to 1.
Abbreviations: PSMA7, proteasome subunit, α-type, 7; RAN, ras-related nuclear protein; RT-PCR, reverse transcriptase-polymerase chain reaction; SD, standard deviation.

Thus, downregulation of PSMA7 and RAN expression by siRNA induces apoptosis in colon cancer cells, results that suggest that PSMA7 and RAN might act as a suppressor of apoptosis in colorectal cancer.

Overexpression of PSMA and RAN in colorectal cancer cell lines and tumor tissues

To investigate the role of PSMA and RAN in colorectal cancer, we analyzed the mRNA expression levels of PSMA7 and RAN by real-time RT-PCR. PSMA7 and RAN mRNA were significantly highly expressed in colorectal cancer cell lines Caco-2 (human colorectal adenocarcinoma), HCT116 (human colorectal carcinoma), HT-29 (human colorectal adenocarcinoma), LoVo (human colorectal adenocarcinoma, derived from supraclavicular lymph node metastatic site) and T84 (human colorectal carcinoma, derived from lung metastatic site), compared with normal colon tissues (Figures 4A, 4B). mRNA expression levels of PSMA7 and RAN in human tumoral colon tissues were higher than those of normal adjacent colon tissues (Figures 4C, 4D). These results indicate that PSMA7 and RAN strongly correlated with colorectal tumorigenesis and malignancy.

Furthermore, PSMA7 was overexpressed in other tumor tissues, especially uterus, stomach, and small intestine tumor tissues (Figure 4C). Similarly, RAN was overexpressed in other tumor tissues, in particular uterus, liver, testis, and stomach tumors and lymphoma tissues (Figure 4D). Thus, PSMA7 and RAN were overexpressed in not only colon tumor tissues but also in other tumor tissues, and PSMA7 and RAN might be involved in the development of multiple cancers.

Correlation of PSMA7 and RAN expression with liver and lung metastases in human colorectal cancer

We next investigated the levels of *PSMA7* and *RAN* expression in human colorectal cancers. The results are summarized in Table 3. PSMA7 showed a borderline significance ($P = 0.076$) for correlation with liver metastasis in colorectal cancer patients. In contrast, no significant correlation between the PSMA7 expression and lung metastasis was found in patients ($P = 0.534$). Decreased expression of RAN showed a significance ($P = 0.023$) for correlation with lung metastasis; however, there is no correlation with liver metastasis ($P = 0.911$). However, to know whether or not the levels of *PSMA7* and *RAN* expression showed correlation with any other clinicopathological features such as depth of invasion, tumor size, lymphatic invasion, or the presence of lymph node metastasis, further analysis is needed.

PSMA7 siRNA and RAN siRNA induce apoptosis *in vivo*

To extend our *in vitro* findings and to determine whether PSMA7 and RAN could be effective therapeutic targets for colorectal cancer, we examined the effect of PSMA7 siRNA and RAN siRNA on an animal model of colon tumors by subcutaneously implanting HT-29 cells into mice. We injected the PSMA7 siRNA #2, RAN siRNA #4, or nontargeting control siRNA (1 nmol per tumor) into tumors that had reached 5–6 mm in diameter seven days after inoculation of HT-29 cells. The mRNA levels of PSMA7 and RAN in the tumors given siRNA were measured. mRNA expression was significantly reduced in mouse tumors 24 hours after treatment with PSMA7 siRNA and RAN siRNA, 40% and 30% reduction relative to nontargeting control siRNA, respectively ($P < 0.05$, Figure 5A).

HT-29 tumors treated with PSMA7 siRNA or RAN siRNA were investigated for apoptotic activity. Three days after siRNA treatment, we performed TUNEL staining which detects apoptotic DNA breaks *in situ*. TUNEL staining of tumor tissue treated with PSMA7 siRNA and RAN siRNA revealed a significant number of apoptotic cells relative to the number in the nontargeting control siRNA treated tumors

Table 3 Correlation of *PSMA7* and *RAN* expression with liver and lung metastases in human colorectal cancer

	No of subjects	*PSMA7*		*RAN*	
	(*n* = 191)	expression	*P*-value	expression	*P*-value
Liver metastasis					
Positive	41	1.108 ± 0.116	0.0762	0.597 ± 0.052	0.9112
Negative	150	0.884 ± 0.043		0.605 ± 0.031	
Lung metastasis					
Positive	29	0.870 ± 0.112	0.5336	0.460 ± 0.064	0.0233
Negative	162	0.943 ± 0.045		0.629 ± 0.029	

Note: Values are mean ± standard error.

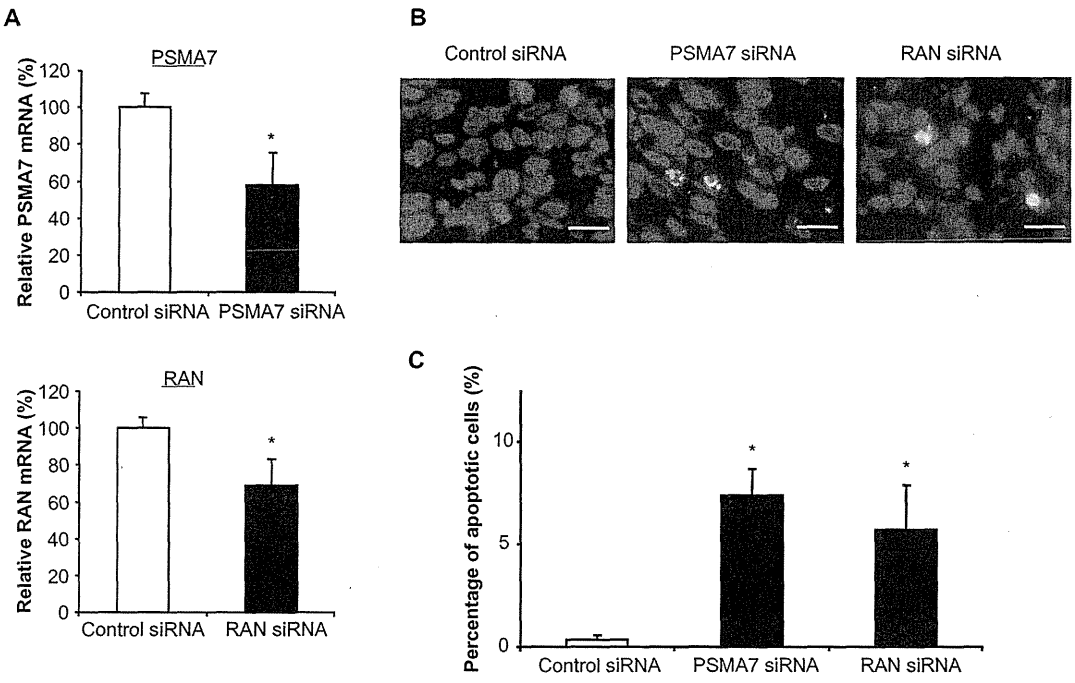

Figure 5 Apoptosis induction by PSMA7 siRNA and RAN siRNA treatment *in vivo*. **A)** Expression of PSMA7 mRNA and RAN mRNA in HT-29 tumors treated with siRNA. ($n = 4$ per group, $^*P < 0.05$). **B)** TUNEL staining of HT-29 tumor tissues treated with siRNA. Scale bar, 20 μm. **C)** TUNEL-positive cells were counted and represented ($n = 3$ per group, $^*P < 0.05$). As a control, nontargeting siRNA was used. Values are mean ± SD.
Abbreviations: PSMA7, proteasome subunit, α-type, 7; RAN, ras-related nuclear protein; SD, standard deviation; siRNA, small interfering RNAs.

($P < 0.05$, Figures 5B, 5C). These results indicate that PSMA7 siRNA and RAN siRNA induce apoptotic cell death *in vivo*.

Discussion

Molecular targeted therapy is one of the most promising approaches in cancer treatment. For cancer researchers it is now possible to understand the molecular mechanisms of the development and progression in many types of cancer. It is expected that many potential new molecular targets will be discovered for cancer therapy. To identify molecular targets for colorectal cancer therapy, we performed a sophisticated strategy using RNAi-based reverse genetics *in vitro* and *in vivo*. RNAi is a cellular mechanism for silencing of gene expression. Following the demonstration of RNAi mediated by siRNA in mammalian cells in 2001,[22] RNAi has provided new powerful tools for biological research and drug discovery. Additionally, therapeutics based on RNAi offers a new class of pharmaceutical drugs. The inhibition of gene expression through RNAi is applicable to all classes of molecular targets, including the "undruggable targets" of traditional pharmaceutical drugs such as small molecule and protein.

First, we carried out a gene expression profiling of subjects with colorectal tumors and selected 97 genes whose expression was elevated in human colorectal cancer tissues as a screening source of molecular targets. This starting from human disease samples has a great advantage, because cultured cells and disease models cannot faithfully reproduce the pathology of cancer. We then analyzed the function of genes using RNAi *in vitro* and *in vivo*. We performed a functional screening of genes by a reverse transfection-based cell transfection array to obtain an unbiased evaluation on the efficacy of a specific siRNA related to apoptosis induction in human colorectal cancer. An unbiased evaluation is important in the discovery of a new and unique target that brings a novel concept of targeted therapy. Our results showed that the siRNA designed for PSMA7 and RAN significantly promoted apoptosis of HT-29 human colon cancer cells. In our next step, we demonstrated *in vivo* proof-of-concept by the administration of siRNA to a colon tumor model. The *in vivo* delivery of PSMA7 siRNA and RAN siRNA markedly induced apoptosis in HT-29 tumors in mice. Finally, we identified PSMA7 and RAN as new molecular targets for an RNAi-based colorectal cancer therapy.

PSMA7 (also known as XAPC7) is a proteasome subunit.[23] The 26S proteasome consist of a 20S proteasome core and two 19S regulatory subunits.[24] The 20S proteasome core

is a barrel-shaped structure arranged in four stacked rings. Of these four rings, two end rings are composed of seven α-subunits, and two central rings are composed of seven β-subunits. PSMA7 is one of the seven proteasome α-subunits of 20S proteasome. PSMA7 interacts specifically with hepatitis B virus X protein (HBX), which is important in the life cycle of the hepatitis B virus (HBV).[25] In addition, PSMA7 has a principal role in regulating activity of the hepatitis C virus (HCV) internal ribosome entry site (IRES), a function essential for HCV replication.[26]

The ubiquitin–proteasome pathway is the main extra-lysosomal system involved in intracellular proteolysis and is critical for the proliferation and survival of all cells.[24,27] In particular cancerous cells, the ubiquitin-proteasome pathway plays an integral role in the mechanisms underlying carcinogenesis and metastasis, including cell cycle regulation, apoptosis, and angiogenesis.[24,27] The cancer cells exploit the proteasome for their own proliferation through the cell cycle by degrading of cell cycle regulatory proteins. Furthermore, the proteasome regulates apoptotic activity via effects on the pro-oncogenic nuclear factor (NF)-κB pathway, which is a transcriptional activator and activated in many types of tumor.[28] Under normal conditions, NF-κB is bound to its inhibitor IκB (IκB) and in an inactive state. The proteasome degrades IκB in response to cellular stresses, and then NF-κB activates transcription of genes for growth factors and apoptosis inhibitors.[24,29,30] Therefore, proteasome is an attractive target for cancer therapy. A dipeptidyl boronic acid proteasome inhibitor, bortezomib, suppresses degradation of IκB by proteasome and blocks NF-kB signaling with resultant apoptosis.[24,27,29] The efficacy of bortezomib is investigated in various types of malignancies including advanced colorectal cancer.[24,31,32] However, the ubiquitin-proteasome pathway is essential for maintenance of cell function in all cells, and the proteasome inhibitor may attack normal cells and cause severe side effects in patients.[33,34] A proteasome inhibitor specific for cancer cells should provide a better treatment with minimal side effects. In this study, among proteasome subunits genes, *PSMA7* is the only gene listed for genes whose expression is elevated in human colorectal cancer tissues. RNAi-mediated specific inhibition of PSMA7 may be a smart colorectal cancer therapy. Although it is impossible at the moment to judge whether PSMA7 silencing inhibited degradation of IκB by proteasome and blocks NF-kB signaling, in fact, our results indicated that PSMA7 siRNA caused apoptosis in HT-29 colon cells and HT-29 tumor tissues. PSMA7 was overexpressed in not only colon tumor tissues but also in other tumor tissues, which suggests that PSMA7 might be a potential target against various types of cancer.

Moreover, PSMA7 is interesting because of the correlation between its expression and the liver metastasis of colorectal cancer. Our study showed that expression of PSMA7 mRNA was elevated in colorectal tumor tissues from subjects with liver metastasis, although no statistical significance was found. Another research group also reported that overexpression of PSMA7 protein associates with liver metastasis in colorectal cancer.[35] PSMA7 may be a predictive marker and a molecular target for liver metastasis from colorectal cancer. Further investigations are needed to confirm the relationship between PSMA7 and colorectal cancer liver metastasis by gene expression profiling on a validation set of colorectal cancer subjects and analysis of PSMA7 expression on a colorectal cancer liver metastatic site at both the mRNA and protein levels.

RAN protein (Ran) is a small GTPase belonging to the Ras superfamily. Ran is essential for the translocation of RNA and proteins through the nuclear pore complex.[36,37] GTPase Ran regulates numerous cellular processes by switching between a GTP-bound and GDP-bound form.[38] Ran is also critical for the regulation of the cell cycle through mitotic spindle assembly and post-mitotic nuclear envelope assembly.[38,39]

It is reported that Ran is a suppressor of Bcl-2-associated X protein (Bax), a pro-apoptotic member of the Bcl-2 family of proteins, and that it inhibits apoptosis induced by the anticancer drug paclitaxel.[40] Furthermore, it is indicated that silencing of Ran in various tumor cell types causes aberrant mitotic spindle formation, mitochondrial dysfunction, and apoptosis.[41,42] Ran is abundantly expressed in most cancer cell lines and cancer tissues.[41] This suggests that Ran is associated with malignant transformation and/or the enhanced proliferation of cancer cells. There is a current finding that most tumor cells, but not normal tissues, become dependent on Ran signaling for cell mitosis.[41] Targeting the Ran signaling pathway may provide a selective anticancer strategy.

This study showed that RAN mRNA was elevated in colon cancer cell lines and tissues, and in some types of tumor tissue. *RAN* silencing using RAN siRNA induced apoptosis in HT-29 colon cancer cells and HT-29 tumor tissues. RAN siRNA can specifically inhibit Ran which is a main molecule of *RAN* signaling, and may be a selective inhibitor against colon cancer.

We identified PSMA7 and RAN as new molecular targets for colorectal cancer therapy using RNAi-based

screening *in vitro* and *in vivo*. In a further study, we are investigating the antitumor activity of PSMA7 siRNA and RAN siRNA in a colon cancer model and a colon cancer liver metastasis model. Induction of apoptosis is one of the main targets for cancer therapy. The inhibitors of PSMA7 and RAN may provide unique anticancer strategies based on novel mechanisms of action. Since the inhibition of gene expression through RNAi is highly specific and applicable to "undruggable targets", RNAi-based therapeutics using PSMA7 siRNA and RAN siRNA is a particularly promising approach for cancer treatment.

Acknowledgments

We thank Ms Ayako Inoue for her excellent technical assistances. This work was supported in part by a Grant-in-Aid for the Third-Term Comprehensive 10-Year Strategy for Cancer Control of Japan; a Grant-in-Aid for Scientific Research on Priority Areas Cancer from the Ministry of Education, Culture, Sports, Science and Technology, and the Program for Promotion of Fundamental Studies in Health Sciences of the National Institute of Biomedical Innovation (NiBio) of Japan. The authors report no conflicts of interest in this work.

References

1. Garcia M, Jemal A, Ward EM, et al. *Global Cancer Facts and Figures 2007*. Atlanta, GA: American Cancer Society, 2007. p. 12–14.
2. National Cancer Center. Tokyo, Japan. Cancer statistics in Japan (2008). Available from http://ganjoho.ncc.go.jp/public/statistics/backnumber/2008_en.html. Accessed July 2, 2009.
3. Hanahan D, Weinberg RA. The hallmarks of cancer. *Cell*. 2000; 100(1):57–70.
4. Baranda J, Williamson S. The new paradigm in the treatment of colorectal cancer: are we hitting the right target? *Expert Opin Investig Drugs*. 2007;16(3):311–324.
5. Köhne CH, Lenz HJ. Chemotherapy with targeted agents for the treatment of metastatic colorectal cancer. *Oncologist*. 2009;14(5):478–488.
6. Ferrara N, Kerbel RS. Angiogenesis as a therapeutic target. *Nature*. 2005;438(7070):967–974.
7. Kim KJ, Li B, Winer J, et al. Inhibition of vascular endothelial growth factor-induced angiogenesis suppresses tumour growth *in vivo*. *Nature*. 1993;362(6423):841–844.
8. Hurwitz H, Fehrenbacher L, Novotny W, et al. Bevacizumab plus irinotecan, fluorouracil, and leucovorin for metastatic colorectal cancer. *N Engl J Med*. 2004;350(23):2335–2342.
9. Wood JM, Bold G, Buchdunger E, et al. PTK787/ZK 222584, a novel and potent inhibitor of vascular endothelial growth factor receptor tyrosine kinases, impairs vascular endothelial growth factor-induced responses and tumor growth after oral administration. *Cancer Res*. 2000;60(8):2178–2189.
10. Drevs J, Hofmann I, Hugenschmidt H, et al. Effects of PTK787/ZK 222584, a specific inhibitor of vascular endothelial growth factor receptor tyrosine kinases, on primary tumor, metastasis, vessel density, and blood flow in a murine renal cell carcinoma model. *Cancer Res*. 2000;60(17):4819–4824.
11. Mellinghoff I. Why do cancer cells become "addicted" to oncogenic epidermal growth factor receptor? *PLoS Med*. 2007;4(10):1620–1622.
12. Henson ES, Gibson SB. Surviving cell death through epidermal growth factor (EGF) signal transduction pathways: implications for cancer therapy. *Cell Signal*. 2006;18(12):2089–2097.
13. Cunningham D, Humblet Y, Siena S, et al. Cetuximab monotherapy and cetuximab plus irinotecan in irinotecan-refractory metastatic colorectal cancer. *N Engl J Med*. 2004;351(4):337–345.
14. Saltz L, Easley C, Kirkpatrick P. Panitumumab. *Nat Rev Drug Discov*. 2006;5(12):987–988.
15. Taylor K, Micha D, Ranson M, Dive C. Recent advances in targeting regulators of apoptosis in cancer cells for therapeutic gain. *Expert Opin Investig Drugs*. 2006;15(6):669–690.
16. Frenzel A, Grespi F, Chmelewskij W, Villunger A. Bcl2 family proteins in carcinogenesis and the treatment of cancer. *Apoptosis*. 2009;14(4):584–596.
17. Klasa RJ, Gillum AM, Klem RE, Frankel SR. Oblimersen Bcl-2 antisense: facilitating apoptosis in anticancer treatment. *Antisense Nucleic Acid Drug Dev*. 2002;12:193–213.
18. Newsom-Davis T, Prieske S, Walczak H. Is TRAIL the holy grail of cancer therapy? *Apoptosis*. 2009;14(4):607–623.
19. Marini P, Denzinger S, Schiller D, et al. Combined treatment of colorectal tumours with agonistic TRAIL receptor antibodies HGS-ETR1 and HGS-ETR2 and radiotherapy: enhanced effects *in vitro* and dose-dependent growth delay *in vivo*. *Oncogene*. 2006;25(37):5145–5154.
20. Honma K, Iwao-Koizumi K, Takeshita F, et al. RPN2 gene confers docetaxel resistance in breast cancer. *Nat Med*. 2008;14(9):939–948.
21. Komori T, Takemasa I, Yamasaki M, et al. Gene expression of colorectal cancer: preoperative genetic diagnosis using endoscopic biopsies. *Int J Oncol*. 2008;32(2):367–375.
22. Elbashir SM, Harborth J, Lendeckel W, Yalcin A, Weber K, Tuschl T. Duplexes of 21-nucleotide RNAs mediate RNA interference in cultured mammalian cells. *Nature*. 2001;411(6836):494–498.
23. Gerards WL, de Jong WW, Boelens W, Bloemendal H. Structure and assembly of the 20S proteasome. *Cell Mol Life Sci*. 1998;54(3):253–262.
24. Adams J. The development of proteasome inhibitors as anticancer drugs. *Cancer Cell*. 2004;5(5):417–421.
25. Huang J, Kwong J, Sun EC, Liang TJ. Proteasome complex as a potential cellular target of hepatitis B virus X protein. *J Virol*. 1996;70(8): 5582–5591.
26. Krüger M, Beger C, Welch PJ, Barber JR, Manns MP, Wong-Staal F. Involvement of proteasome alpha-subunit PSMA7 in hepatitis C virus internal ribosome entry site-mediated translation. *Mol Cell Biol*. 2001;21(24):8357–8364.
27. Hoeller D, Dikic I. Targeting the ubiquitin system in cancer therapy. *Nature*. 2009;458(7237):438–444.
28. Karin M. Nuclear factor-B in cancer development and progression. *Nature*. 2006;441(7092):431–436.
29. Richardson PG, Mitsiades C, Hideshima T, Anderson KC. Proteasome inhibition in the treatment of cancer. *Cell Cycle*. 2005;4(2):290–296.
30. Palombella VJ, Rando OJ, Goldberg AL, Maniatis T. The ubiquitin-proteasome pathway is required for processing the NF-kappa B1 precursor protein and the activation of NF-kappa B. *Cell*. 1994;78(5): 773–785.
31. Cusack JC Jr, Liu R, Houston M, et al. Enhanced chemosensitivity to CPT-11 with proteasome inhibitor PS-341: implications for systemic nuclear factor-kappaB inhibition. *Cancer Res*. 2001;61(9):3535–3540.
32. Pitts TM, Morrow M, Kaufman SA, Tentler JJ, Eckhardt SG. Vorinostat and bortezomib exert synergistic antiproliferative and proapoptotic effects in colon cancer cell models. *Mol Cancer Ther*. 2009;8(2):342–349.
33. Voortman J, Giaccone G. Severe reversible cardiac failure after bortezomib treatment combined with chemotherapy in a non-small cell lung cancer patient: a case report. *BMC Cancer*. 2006;6:129.
34. Perfetti V, Palladini G, Brunetti L, et al. Bortezomib-induced paralytic ileus is a potential gastrointestinal side effect of this first-in-class anticancer proteasome inhibitor. *Eur J Gastroenterol Hepatol*. 2007;19(7):599–601.
35. Hu XT, Chen W, Wang D, et al. The proteasome subunit PSMA7 located on the 20q13 amplicon is overexpressed and associated with liver metastasis in colorectal cancer. *Oncol Rep*. 2008;19(2):441–446.

36. Kuersten S, Ohno M, Mattaj IW. Nucleocytoplasmic transport: Ran, beta and beyond. *Trends Cell Biol.* 2001;11(12):497–503.
37. Pemberton LF, Paschal BM. Mechanisms of receptor-mediated nuclear import and nuclear export. *Traffic.* 2005;6(3):187–198.
38. Joseph J. Ran at a glance. *J Cell Sci.* 2006;119(Pt 17):3481–3484.
39. Hetzer M, Gruss OJ, Mattaj IW. The Ran GTPase as a marker of chromosome position in spindle formation and nuclear envelope assembly. *Nat Cell Biol.* 2002;4(7):E177–E184.
40. Woo IS, Jang HS, Eun SY, et al. Ran suppresses paclitaxel-induced apoptosis in human glioblastoma cells. *Apoptosis.* 2008;13(10):1223–1231.
41. Xia F, Lee CW, Altieri DC. Tumor cell dependence on Ran-GTP-directed mitosis. *Cancer Res.* 2008;68(6):1826–1833.
42. Morgan-Lappe SE, Tucker LA, Huang X, et al. Identification of Ras-related nuclear protein, targeting protein for xenopus kinesin-like protein 2, and stearoyl-CoA desaturase 1 as promising cancer targets from an RNAi-based screen. *Cancer Res.* 2007;67(9):4390–4398.

International Journal of General Medicine

Dovepress

Publish your work in this journal

The International Journal of General Medicine is an international, peer-reviewed open-access journal that focuses on general and internal medicine, pathogenesis, epidemiology, diagnosis, monitoring and treatment protocols. The journal is characterized by the rapid reporting of reviews, original research and clinical studies across all disease areas.

A key focus is the elucidation of disease processes and management protocols resulting in improved outcomes for the patient.The manuscript management system is completely online and includes a very quick and fair peer-review system. Visit http://www.dovepress.com/testimonials.php to read real quotes from published authors.

Submit your manuscript here: http://www.dovepress.com/international-journal-of-general-medicine-journal

© The American Society of Gene & Cell Therapy

Systemic Delivery of Synthetic MicroRNA-16 Inhibits the Growth of Metastatic Prostate Tumors via Downregulation of Multiple Cell-cycle Genes

Fumitaka Takeshita[1], Lubna Patrawala[2,3], Mitsuhiko Osaki[1,4], Ryou-u Takahashi[1], Yusuke Yamamoto[1,5], Nobuyoshi Kosaka[1], Masaki Kawamata[1], Kevin Kelnar[2,3], Andreas G. Bader[2,3], David Brown[2,3] and Takahiro Ochiya[1]

[1]Section for Studies on Metastasis, National Cancer Center Research Institute, Tokyo, Japan; [2]Asuragen, Inc., Austin, Texas, USA; [3]Mirna Therapeutics, Inc., Austin, Texas, USA; [4]Division of Molecular Genetics and Biofunction, Tottori University Graduate School of Medical Science, Tottori, Japan; [5]Department of Biology, School of Education, Waseda University, Tokyo, Japan

Recent reports have linked the expression of specific microRNAs (miRNAs) with tumorigenesis and metastasis. Here, we show that microRNA (miR)-16, which is expressed at lower levels in prostate cancer cells, affects the proliferation of human prostate cancer cell lines both *in vitro* and *in vivo*. Transient transfection with synthetic miR-16 significantly reduced cell proliferation of 22Rv1, Du145, PPC-1, and PC-3M-luc cells. A prostate cancer xenograft model revealed that atelocollagen could efficiently deliver synthetic miR-16 to tumor cells on bone tissues in mice when injected into tail veins. In the therapeutic bone metastasis model, injection of miR-16 with atelocollagen via tail vein significantly inhibited the growth of prostate tumors in bone. Cell model studies indicate that miR-16 likely suppresses prostate tumor growth by regulating the expression of genes such as *CDK1* and *CDK2* associated with cell-cycle control and cellular proliferation. There is a trend toward lower miR-16 expression in human prostate tumors versus normal prostate tissues. Thus, this study indicates the therapeutic potential of miRNA in an animal model of cancer metastasis with systemic miRNA injection and suggest that systemic delivery of miR-16 could be used to treat patients with advanced prostate cancer.

Received 21 May 2009; accepted 12 August 2009; published online 8 September 2009. doi:10.1038/mt.2009.207

INTRODUCTION

Advanced prostate cancer is frequently difficult to treat and causes substantial symptoms, including severe pain from metastasis to bone or other sites. Numerous experimental therapeutics are being pursued in clinical trials and offer some hope of improved treatments, but most have so far demonstrated only modest results.

Mounting evidence suggests that the altered expression of specific microRNA's (miRNA's) accuracy contributes to the development of a variety of cancers. Cancer types including prostate cancers can be classified based on their distinct miRNA expression profiles.[1–5]

MiRNAs have been implicated in prostate cancer. Volinia *et al.* identified >40 miRNAs with expression levels that were significantly different in prostate tumors versus normal prostate tissue.[5] Furthermore, the need for additional therapies in metastasis due to hormone-refractory prostate cancer is considerable. Mattie *et al.* found that miRNA expression in human prostate cancer cell lines could distinguish androgen hormone–insensitive PC3 from hormone-sensitive LNCaP cells.[6] LNCaP cells showed upregulation of microRNA (miR)-200c, miR-195, and several let-7 family members, whereas miR-10a, miR-27b, miR-221, miR-222, and mir-210 were lower than in PC3. The serum prostate-specific antigen is the most useful tumor marker for diagnosis and monitoring of prostate cancer. However, its low specificity in distinguishing prostate carcinoma from benign prostatic hyperplasia limits its use as an early detection biomarker. Investigators used custom designed arrays to compare the expression profiles of 319 miRNAs in prostate tumors, cancer cell lines, xenografts, and benign prostatic hyperplasia.[7] MiRNAs could be used to cluster the androgen receptor status of cell lines and xenografts. Among a small set of benign prostatic hyperplasia, hormone refractory, and untreated prostate carcinomas they found 51 differentially expressed miRNAs, 37 of which were downregulated. MiRNAs in this set accurately clustered the benign prostatic hyperplasia, untreated and hormone-refractory prostate carcinomas providing evidence that miRNA expression profiles are altered by changes in disease status. More recently, Bonci *et al.* showed that miR-15a and miR-16-1 cluster inhibit the tumor cell proliferation and invasion via targets CCND1 (cyclinD1), WNT3A, and BCL2 in prostate cancer cell line and clinical samples.[8] These miR-15a and miR-16-1 were coded on chromosome 9 13q14. In this region, loss of heterogeneity was detected in chronic lymphocytic leukemia[9] and prostate cancer patients.[10] These results suggest that miR-15a and/or miR-16 could be a novel target for prostate cancer therapy.

To supplement the expression studies that have been published for prostate cancer, we used a library of synthetic miRNAs

Correspondence: Takahiro Ochiya, Section for Studies on Metastasis, National Cancer Center Research Institute, 1-1, Tsukiji 5-chome, Chuo-ku, Tokyo 104-0045, Japan. E-mail: tochiya@ncc.go.jp

© The American Society of Gene & Cell Therapy

to identify the small RNAs that alter the proliferation of prostate cancer cells. Among the miRNAs that were identified in a functional screen featuring 22Rv1 prostate cancer cells was miR-16, an miRNA that has been implicated in chronic lymphocytic leukemia[1,11,12] and prostate cancer.[8,10] Our studies of miR-16 revealed that it has the capacity to affect the proliferation of a variety of human-derived prostate cancer cells. For the evaluation of miRNA therapy for bone metastasis of prostate cancer, the mouse model of bone-metastatic prostate cancer using bioluminescence-based *in vivo* imaging analysis was selected. We have already established small-interfering RNA (siRNA) molecules that can be delivered to tumor cells in a bone metastatic site using an atelocollagen delivery method.[13] The properties of synthetic miRNA molecules are similar to synthetic siRNA; therefore, it is speculated that synthetic miRNA can also be used for systemic treatment mediated by atelocollagen. In this article, the systemic delivery of synthetic miR-16 using atelocollagen inhibited bone-metastatic human prostate tumor growth in a mouse bone site. We further analyzed the altered expression of cancer-related genes in miR-16-transfected prostate cancer cells and verified that genes associated with cell-cycle progression were mostly affected by miR-16. These results suggest a therapeutic potency of miR-16 in bone-metastatic prostate cancer.

RESULTS

Effect of miR-16 on proliferation of human prostate cancer cell lines

22Rv1 prostate cancer cells were transiently transfected in triplicate with individual synthetic mimics for ~200 miRNAs. Three days after transfection, the cells were monitored for proliferation and apoptotic activity. Among the most active miRNAs identified in the functional screen was miR-16, which reduced the proliferation of the prostate cancer cells by 25% and increased apoptosis by 40% (data not shown). Follow-up studies for measuring the proliferation; using the alamar blue assay with another prostate cancer cell line, PC-3M-luc, revealed that miR-16 reduces proliferation by 60% (**Figure 1a**) relative to the cells transfected with a negative control (NC) miRNA. Further studies of the antiproliferative effect of miR-16 on prostate cancer cells revealed that synthetic miRNA can significantly affect the expansion of cultured 22Rv1, PPC-1, and Du145 cells (**Figure 1a**). The only prostate cancer cell line that proved to be unaffected by the transfection of miR-16 was LNCaP (**Figure 1a**). The amount of miR-16 in the PC-3M-luc cells transfected with synthetic miR-16 was >500-fold higher than that in the control cells (**Figure 1b**). This result suggests that the induced increase of intracellular miR-16 concentrations is capable of suppressing the proliferation of the prostate cancer cells.

miR-16 expression levels in prostate cancer cell lines

Although four of the five prostate cancer cell lines exhibit significant reductions in proliferation following transfection with synthetic miR-16, it is interesting that there is a variation in the level of the effect. To address whether this might be due to variation in the levels of endogenous miR-16 in the various cell lines, we used quantitative reverse transcription (qRT)-PCR to measure the relative abundance of mature miRNA. As shown in **Figure 1c**, most of the cell lines expressed miR-16 at reduced levels. The extent

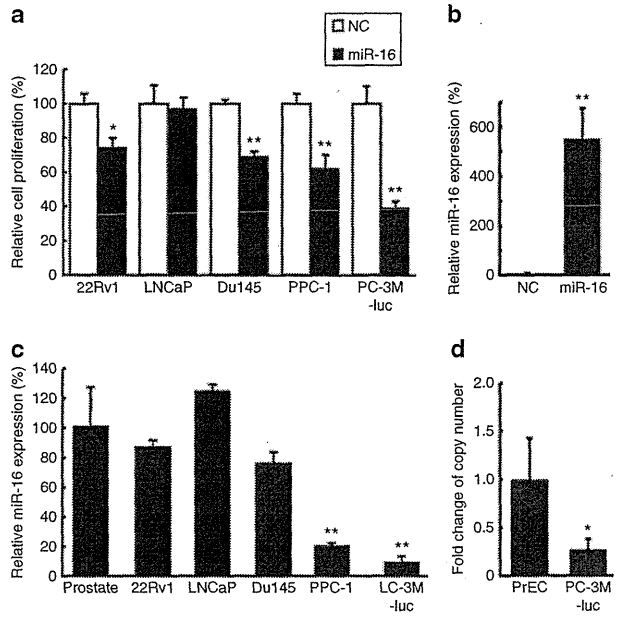

Figure 1 The expression and function of miR-16 in human prostate cancer cell lines. (**a**) Effect of miR-16 on proliferation of human prostate cancer cell lines. Percent (%) proliferation values were normalized to values from cells treated with negative control (NC) microRNA (miRNA). Data represent the mean (n = 4) ± SD *P < 0.05, **P < 0.01 versus NC miRNA. (**b**) The amount of miR-16 in PC-3M-luc cells transfected with synthetic miR-16. The cellular level of miR-16 was detected by quantitative PCR. The data represent the mean (n = 3) ± SD **P < 0.01 versus NC miRNA. (**c**) Expression level of miR-16 in human prostate cancer cell lines. The relative expression of miR-16 for each of the cell lines was calculated by comparing the level in normal prostate tissue samples. The data represent the mean (n = 3) ± SD **P < 0.01 versus normal human prostate tissue. (**d**) The copy number change of the miR-16 loci on chromosome 13q14 in PC-3M-luc cells. The copy number of miR-16 genes were quantified by real-time PCR with genomic DNA. Cultured normal human prostate epithelial cells (PrEC) was used as the control for this experiment for comparison to the PC-3M-luc cells. The data represent the mean (n = 3) ± SD *P < 0.05 versus PrEC.

of downregulation correlated with the phenotypic response in these cell lines: *e.g.*, PPC-1 and PC-3M-luc cells, which showed the strongest response to miR-16, had the lowest levels of endogenous miR-16 (**Figure 1a**). The DNA copy numbers on chromosome 13q14, a genomic region that is frequently deleted in chronic lymphocytic leukemia and prostate cancer[14] in the PC-3M-luc cells were reduced to half that of normal prostate cells (**Figure 1d**). However, because the DNA sequence data did not show any mutations on chromosomes coding miR-16 of other copy in the PC-3M-luc cells (data not shown), the remarkable reduction of miR-16 expression might be invoked by a combination of DNA copy number alteration and other factors to affect the expression. LNCaP cells, which showed no response to the miR-16 mimic, were the only cells that tend to have higher miR-16 expression levels than the normal prostate (**Figure 1c**). Additionally, the transfection of miRNAs, which are not downregulated in PC-3M-luc cells, such as miR-10a and miR-188, did not inhibit the growth of PC-3M-luc cells (data not shown). The expression and function data suggest that reduced expression of miR-16 is critical for sustained proliferation in some prostate

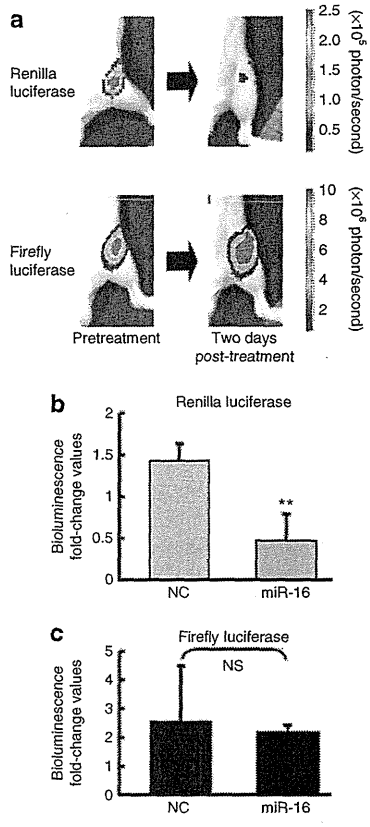

Figure 2 Evaluation of delivery for synthetic microRNA (miRNA) molecules to tumors in bone. A dual-luciferase expressing PC-3M cells that have 3′-UTR of Bcl2 under the renilla luciferase gene, PC-3M-luc/Rluc-Bcl2 3′UTR cells, were generated. These cells were used for dual assay system, for monitoring of tumor growth by firefly luciferase, for monitoring of delivery efficacy of synthetic miR-16 by renilla luciferase. (**a**) Representative images of bone metastasis in the femur of mice. To examine the efficacy of synthetic miR-16 in tumor cells, PC-3M-luc/Rluc-Bcl2 3′UTR cells were injected into the heart of nude mice. Nine weeks after tumor injection, bioluminescence from renilla luciferase was detected. Intravenous injection of miR-16 complexed with atelocollagen suppressed the expression of renilla luciferase (top). In contrast, bioluminescence from firefly luciferase was not affected (bottom). (**b**) Normalized fold change (2 days post/pre-miR-16 administration) of bioluminescence emitted from whole body of mice. This figure is graphically shown of the results of **Figure 2a** by fold change of photon counts. Data represent the mean (n = 3) ± SD *P < 0.01 versus NC miRNA. NS, not significant. NC, negative control.

cancer cell lines and that reintroduction of miR-16 can interfere with that phenotype.

Evaluation of miRNA delivery to bone-metastatic tumors in mice

In order to assess the capacity of the synthetic miR-16 to affect prostate tumor growth in mice, we chose to use a mouse model featuring PC-3M-luc cells that have the capacity to form prostate tumors in the bones of mice.[13,15,16] To evaluate that atelocollagen can efficiently deliver synthetic miRNA molecules to metastatic prostate tumors in bone, we generated a PC-3M-luc metastatic prostate cancer cell line stably expressing the renilla luciferase gene fused to the 3′UTR of Bcl2, a validated miR-16 target (**Supplementary Figure S1a**).[17] Thus, this newly engineered cell line PC-3M-Fluc/Rluc-Bcl2 3′UTR expresses both firefly and renilla luciferase, the later of which is under control of miR-16 (**Supplementary Figure S1b**). As expected, transfection of cultured PC-3M-Fluc/Rluc-Bcl2 3′UTR cells with 30 nmol/l of miR-16 deceased the luminescence derived from renilla luciferase (**Supplementary Figure S1c**). To monitor atelocollagen-mediated delivery of miR-16 in the animal, PC-3M-luc/Rluc-Bcl2 3′UTR cells were intracardiac injected into mice and allowed the tumor cells to deposit in the bone. Nine weeks after implantation, the mice were tail-vein injected with 50 μg of miR-16 mimic that was complexed with atelocollagen. Mice injected with the miR-16/atelocollagen complex produced <50% renilla luciferase from tumors in the bone than they produced before treatment (**Figure 2a,b**). The signal from the firefly luciferase that represents tumor growth was unaffected by the synthetic miR-16, indicating that the inhibition observed for renilla luciferase was due to the binding of injected synthetic miR-16 to the 3′UTR of Bcl2. Synthetic miR-16 was detected in tumor tissue at >20 pg/mg tissue when injected systemically and it was observed to persist in tumors for 3 days after injection (data not shown). Thus, our dual-luciferase prostate cancer xenograft model clearly showed that atelocollagen can efficiently deliver active miRNAs into metastatic tumors in mice.

Inhibition of tumor growth in bone tissues in mice with systemic miR-16 treatment

To assess the therapeutic potential of the miR-16/atelcollagen complexes, prostate tumors were initiated in the bones of mice by intracardiac injection of PC-3M-luc cells. A 50 μg of miR-16 mimic complexed with atelocollagen was administered intravenously into mice at 4, 7, and 10 days after prostate tumor initiation (**Supplementary Figure S2**). The development of tumor in the bone was monitored *in vivo* by bioluminescent imaging. At the end of the experiment on day 28, mice treated with the NC miRNA/atelocollagen complex showed the presence of tumor in the thorax, jaws, and/or legs of mice frequently (**Figure 3a**). In contrast, the mice injected with miR-16/atelocollagen complex exhibited no increase in luminescence during the same observation period. There are significant differences between NC and miR-16 treatment groups on day 28 (P < 0.05) (**Figure 3b**). Histopathological analysis also revealed that growth of PC-3M-luc cells in the bone tissues of mice was significantly inhibited by the miR-16 treatment (**Figure 3c**). These data suggest that atelocollagen-mediated systemic delivery of miR-16 could be a novel strategy for inhibition of prostate tumor growth in the bone tissues.

miR-16 expression in human prostate tissues

We used qRT-PCR to quantify miR-16 levels in the tumors and normal adjacent tissues of seven prostate cancer patients as well as four additional prostate tumors. The relative expression level of miR-16 in each of the samples was calculated by comparing to the average normalized miR-16 levels in prostate samples from three normal donors. The average relative expression of miR-16 in the seven prostate normal adjacent samples was 95% with a standard deviation of 16% and the eleven prostate tumors was 73% with a standard deviation of 28% (**Figure 4**). There is a trend toward lower miR-16 expression in prostate tumors versus normal

© The American Society of Gene & Cell Therapy

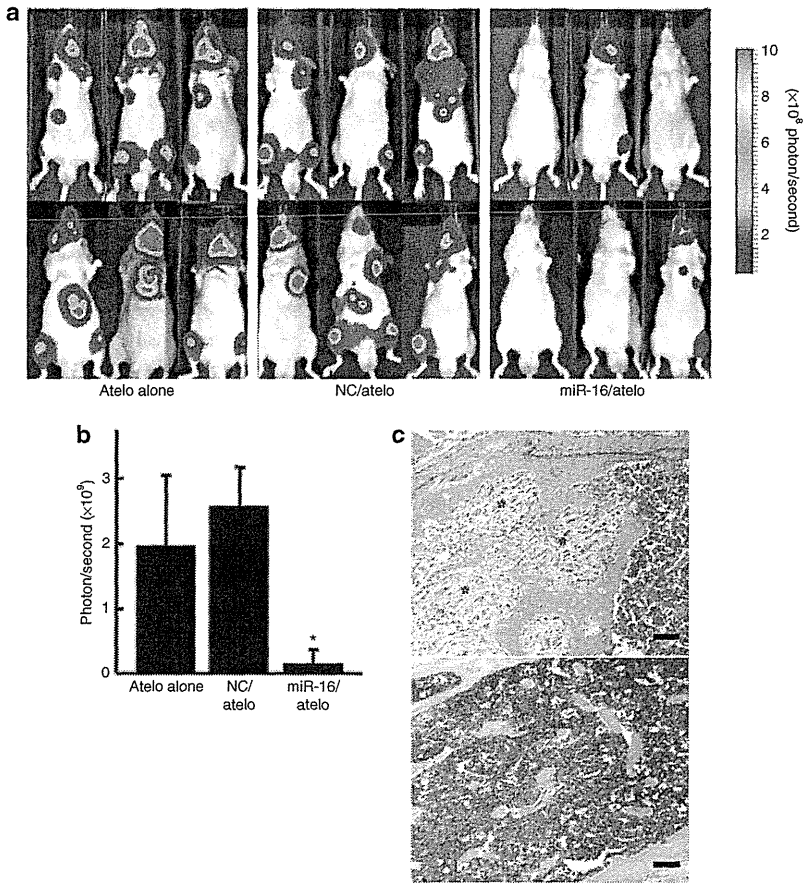

Figure 3 Inhibition of metastatic tumor growth in bone tissues by the atelocollagen-mediated miRNA treatment. Mice were injected with 2×10^6 PC-3M-luc-C6 cells into the left heart ventricle on day zero. The miR-16 and NC miRNA (50 μg) with 0.05% atelocollagen (Atelo) or Atelo alone in a 200 μl volume were injected into the tail vein on days 4, 7, and 10 after tumor injection. At the end of the experiment on day 28, the metastasis was evaluated by IVIS imaging and confirmed by subsequent necropsy. (**a**) All mice used in this experiment on day 28 were shown. There was an increase in luminescence in mice treated with atelocollagen alone and NC miRNA whereas the miR-16/atelocollagen-treated groups had no or low increase in luminescence during the same observation period. (**b**) Quantitation of bioluminescence emitted from whole body of mice on day 28. Data represent the mean ($n = 6$) ± SD *P<0.05 versus other groups. (**c**) Histopathological analysis confirmed micrometastasis in the tibia of nontreated mice (upper). Metastatic lesions are indicated by asterisk mark. In the miR-16-treated mice, any micrometastasis was not observed (lower). Bar = 100 μm.

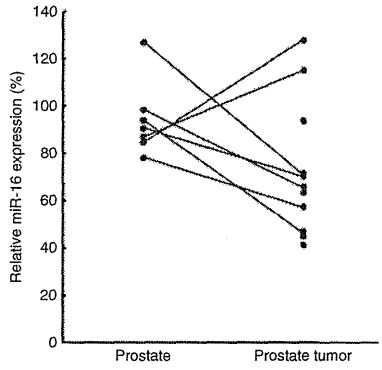

Figure 4 Clinical association of miR-16 expression with prostate cancer. The qRT-PCR analysis to quantify miR-16 levels in the tumors and normal adjacent tissues of seven prostate cancer patients and four additional prostate tumors was performed. The P value calculated by Student's t-test for the two sample sets was 0.08.

prostate tissues, but this trend did not reach statistical significance (Figure 4).

mRNA array analysis following transfection of synthetic miR-16

To get insight into the antioncogenic mechanism of miR-16, we transfected PC-3M-luc cells with the miR-16 mimic and analyzed the expressions of mRNA using mRNA array analysis. Exogenously, miR-16 might directly affect the mRNA levels of the target genes and indirectly affect the expression of genes that are downstream of these direct targets.[18] To identify the pathways that could be affected both directly and indirectly by miR-16, total RNA was isolated from the cells 72 hours after miR-16 transfection. The mRNA array data for the miR-16-transfected samples were compared to the NC miRNA–transfected samples (**Supplementary Table S1**). Fold-differential and P value calculations were used to select 285 mRNAs whose expression levels were significantly altered in the miR-16-transfected samples. A selection of genes suppressed

Table 1 Genes suppressed by miR-16

Gene title	Fold-change (miR-16 versus NC)[a]	*P* value[a]	Cellular process[b]
Aurora kinase B	0.61	2.83×10^{-5}	Chromosomal stability
BUB1	0.58	4.34×10^{-8}	Chromosomal stability
BUBR1	0.61	5.73×10^{-6}	Chromosomal stability
Cyclin D3	0.71	1.30×10^{-6}	Cell cycle
CDK1	0.58	4.99×10^{-7}	Cell cycle
CDK2	0.65	2.35×10^{-5}	Cell cycle
Double parked, DUP	0.76	4.07×10^{-5}	Chromosomal stability
Cks1	0.63	4.71×10^{-6}	Cell cycle
Forkhead box M1	0.61	8.19×10^{-6}	Transcription
Polo-like kinase 1	0.72	1.42×10^{-3}	Chromosomal stability
TACC1	0.76	1.56×10^{-4}	Cell cycle
TACC3	0.64	1.51×10^{-5}	Cell cycle
Thymidylate synthetase	0.56	2.50×10^{-8}	Nucleotide synthesis

Abbreviations: miRNA, microRNA; NC, negative control.
[a]Fold change and *P* value were determined by calculating the ratio of global normalized signals from miR-16 transfected cells to NC miRNA–transfected cells in expression array analysis. [b]Genes are clustered by cellular process, according to their gene ontology classification.

Table 2 Classes of genes affected by miR-16

Functional class	Count[a]	%[b]	*P* value[c]
M phase of mitotic cell cycle	20	12.7	9.60×10^{-19}
DNA metabolism	21	13.3	4.00×10^{-7}
Cytoskeleton organization and biogenesis	16	10.1	8.00×10^{-7}
Cytoskeleton-dependent intracellular transport	9	5.7	6.90×10^{-6}
Regulation of progression through cell cycle	15	9.5	2.50×10^{-5}
Mitotic sister chromatid segregation	4	2.5	6.10×10^{-4}
Establishment of cellular localization	13	8.2	4.10×10^{-3}
Mitotic spindle organization and biogenesis	3	1.9	5.50×10^{-3}
Regulation of progression through mitotic cell cycle	3	1.9	8.10×10^{-3}

[a]The number of genes affected in functional pathway. [b]The percentage calculated from the number of genes affected in functional pathway divided by the number of genes included on the arrays. [c]The significance of the appearance of the functional class in affected genes was calculated as *P* value using DAVID 2.0 software.

by miR-16 is listed in **Table 1**. Pathway analysis combining the Kyoto Encyclopedia of Genes and Genomes[19–21] and Database for Annotation, Visualization, and Integrated Discovery[22] was used to analyze the list of genes with altered expression to determine if there was a significant enrichment of genes associated with any known cellular pathways (**Table 2**). Overall, the statistical enrichment of pathways was moderately low, suggesting that no single pathway or network was specifically and vigorously responsive to the treatment. However, for those pathways that were considered enriched, a few strong underlying themes emerged. The gene lists were enriched for functions related to cell division and control of the cell cycle (**Table 2**). The functions associated with cell-cycle control were most enriched in miR-16-affected genes and these 12 genes that cover G1, S, G2, and M phase of cell cycle are mapped into the Kyoto Encyclopedia of Genes and Genomes Pathway Cell Cycle Map (**Supplementary Figure S3**). Thus, these data suggest that strong inhibition of prostate tumor growth in bone tissues of our animal model was due to downregulation of a key component of cell-cycle genes.

DISCUSSION

The likely involvement of miR-16 in the development of prostate cancer is apparent on multiple levels. The loss of the genomic locus at 13q14 that encompasses the miR-16-1 gene has been reported to be highly associated with human prostate cancer progression.[14] Dong *et al.* suggested loss of heterogeneity at 13q14 is associated with clinically significant high-grade and high-stage prostate cancers[10] with ties to both metastasis and tumor initiation.[23] Consistent with its genomic location, our qRT-PCR results showed that the miR-16 is significantly reduced in most prostate tumors and cultured prostate cancer cells relative to normal prostate tissues.

Based on our studies with cultured prostate cancer cells, the reduced expression of miR-16 is likely necessary to maintain high rates of proliferation. The relationship between miR-16 and apoptosis likely stems from the miRNA's apparent role in regulating BCL2 expression.[17] Our previous data also showed that the transfection of miR-16 into 22Rv1 prostate cancer cells induced apoptosis (F. Takeshita *et al.*, unpublished results). Although increased apoptosis is likely to be at least partially responsible for the reduced proliferation rates that we observed in miR-16-transfected PC-3M-luc cells, it appears that the small RNA also affects cell-cycle progression by regulating the expression of multiple cell-cycle genes. The transfection of prostate cancer cells with synthetic miR-16 reduced the expression of genes like *Cyclin D3*, *CDK1*, *CDK2*, *Cks1*, *TAAC1*, and *TAAC3* that play roles in regulating cell-cycle progression. The apparent capacity of miR-16 to simultaneously regulate cell cycle and apoptosis points to the likely importance of the small RNA in maintaining normal cell function and underscores the influence that the altered expression of the miRNA likely has on tumorigenesis.

The importance of miRNAs like miR-16 as tumor suppressors is becoming increasingly clear. Myriad array and qRT-PCR studies have revealed that the expression levels of specific miRNAs are reduced in the tumors of patients with a variety of cancers.[4,5] When transfected into cancer cells, many of these miRNAs affect proliferation, viability, cell cycle, or apoptosis[24,25] and affect the expression of multiple known oncogenes.[17,18,26–28] Although the growth inhibition of LNCaP cells was not induced by transfection of miR-16 in our study, Bonci *et al.* showed that such inhibition of LNCaP cells was induced by transduction of the *miR-15a-miR-16-1* cluster by lentiviral vector.[8] This discrepancy indicated that the growth inhibition of LNCaP might be induced mainly by induction of miR-15a, further careful studies are needed, considering any clinical application of miR-16.

The clinical application of these naturally occurring tumor suppressors represents a major opportunity for the future treatment

© The American Society of Gene & Cell Therapy

of cancer patients. As with other oligonucleotide-based therapies, realizing the potential of therapeutic miRNAs will require an effective delivery technology. In a previous study, we showed that intravenous injections of EZH2 and p110α siRNA complexed with atelocollagen inhibited the tumor growth in bone tissues of the mouse model.[13] These results showed that an atelocollagen-mediated systemic delivery of siRNA could reach tumor cells at metastatic sites and inhibit tumor growth *in vivo*. As demonstrated here, atelocollagen facilitates the accumulation of enough synthetic miRNA in the cancers cells of an existing prostate tumor to affect the expression of a target gene. Furthermore, the combination of synthetic miR-16 and atelocollagen strongly inhibited the development of human prostate tumors in the bones of mice. Interestingly, the effect of miR-16 appeared to be restricted to the prostate cancer cells, as the miR-16 treated mice showed no notable side effects. Follow-up studies featuring the treatment of larger tumors and more extensive toxicity studies will be required to demonstrate the therapeutic potential of atelocollagen-miR-16; however, these early results are extremely encouraging.

MATERIALS AND METHODS

Cell culture. The human prostate cell line 22Rv1, LNCaP, DU145, and PPC-1 cells were obtained from American Type Culture Collection (Manassas, VA) and maintained in RPMI 1640 medium containing 10% fetal bovine serum. The PC-3M-luc cells continuously expressing firefly luciferase (Xenogen, Alameda, CA) were maintained in RPMI 1640 medium supplemented with 10% fetal bovine serum and 0.2 mg/ml zeocin (Invitrogen, Carlsbad, CA). For construction of 3′-UTR–renilla luciferase plasmid and reporter assays, the segment of 3′-UTR of *Bcl2* gene was amplified by PCR using genomic DNA from normal human prostate epithelial cells (CT-2555; Lonza Walkersville, Walkersville, MD) as reported.[17] The PCR product was inserted into the pGL4.75[HRuc/CMV] vector (Promega, Madison, WI), using *XbaI* site immediately downstream from the stop codon of renilla luciferase (pGL4.75[HRuc/CMV]-Bcl2 3′UTR). For reporter assays, PC-3M-luc-C6 cells were transfected with 2 μg of pGL4.75[HRuc/CMV]-Bcl2 3′UTR using LipofectAMINE 2000 (Invitrogen). Stable transfectants were selected in hygromycine (0.2 mg/ml; Invitrogen) and bioluminescence was used to screen transfected clones for renilla and firefly luciferase gene expression using dual-luciferase assay system (Promega), intensity of renilla luciferase was normalized by firefly luciferase. Clones expressing the both luciferase gene were named PC-3M-luc/Rluc-Bcl2 3′UTR. The cells were maintained *in vitro* at 37 °C in a humidified atmosphere of 5% CO_2.

Transfection with synthetic miR-16 and assay of cellular proliferation. Synthetic hsa-miR-16 (Pre-miR-hsa-miR-16; Ambion, Austin, TX) or NC miRNA (Pre-miR microRNA Precursor Molecule-Negative Control #2, cat. no. AM17111; Ambion) was delivered via lipid-based reverse transfection with 30 nmol/l final concentration of miRNA as described previously.[29] As a control for inhibition of cellular proliferation, siRNA against the motor protein kinesin 11, also known as Eg5, was used. Eg5 is essential for cellular survival of most eukaryotic cells and a lack thereof leads to reduced cell proliferation and cell death.[30] siEg5 was used in lipid-based transfection following the same experimental parameters that apply to miRNA. We observed 50–70% growth inhibition in all cell lines used in this study. Percent (%) proliferation values from the alamar blue assay (Invitrogen) were normalized to values from cells treated with NC miRNA.

Quantitative RT-PCR of miR-16. Human cultured cell line RNA was isolated using the ISOGEN (Wako Chemical, Tokyo, Japan). MiRNA-specific complementary DNA was generated using the TaqMan MicroRNA RT Kit (Applied Biosystems, Foster City, CA) and the miRNA-specific RT primer from the TaqMan Micro RNA Assay (Applied Biosystems). The expression of the U6 small nuclear RNA was used as an internal normalization control. miRNA levels were also measured by using the miRNA-specific probe included with TaqMan Micro RNA Assay on a Real-Time PCR System 7300 and SDS software (Applied Biosystems).

Quantitative PCR of miR-16 loci on chromosome 13q14. Genomic DNAs were extracted from PC-3M-luc and prostate epithelial cells using DNAeasy (Qiagen, Valencia, CA). Quantitative PCR for the miR-16 loci on chromosome 13q14 was performed using Platinum SYBR Green qPCR SuperMix-UDG (Invitrogen) and primer sequences were 5′-GCA GCA CAG TTA ATA CTG GA-3′ and 5′-ATA GCT CTT ATG ATA GCA AT-3′. The house keeping gene, *RNase P* was also quantified as a control reference gene using Platinum Quantitative PCR SuperMix-UDG (Invitrogen) and TaqMan RNase P Detection Reagents Kit (Applied Biosystems). The reactions were incubated at 50 °C for 2 minutes, then heated to 95 °C for 2 minutes followed by 45 cycles of 15 seconds at 95 °C, and 30 seconds at 60 °C.

Evaluation of miRNA delivery to bone-metastatic tumors in mice. Animal experiments in this study were performed in compliance with the guidelines of the Institute for Laboratory Animal Research, National Cancer Center Research Institute. Seven- to ten-week-old male Balb/c athymic nude mice (CLEA Japan, Shizuoka, Japan) were anesthetized by exposure to 3% isoflurane on day zero and subsequent days. On day zero of the experiments, to generate a bone-metastatic human prostate cancer model, the anesthetized animals were injected with 2×10^6 PC-3M-luc/Rluc-Bcl2 3′UTR cells suspended in 100 μl sterile Dulbecco's phosphate-buffered saline into the left heart ventricle.[13,15,16] For *in vivo* imaging, the mice were injected with ViviRen (5 mg/kg; Promega) by intravenous tail vein injection and imaged immediately to count the photons from animal whole bodies using the IVIS imaging system (Xenogen). After the bioluminescence from renilla luciferase disappeared, photons from firefly luciferase were counted as described previously.[13]

Preparation of complex with miR-16 and atelocollagen. For preparing the complexes of miRNA and atelocollagen (Koken, Tokyo, Japan), an equal volume of atelocollagen (0.1 % in phosphate-buffered saline at pH 7.4) and miRNA solution were combined and mixed by rotating for 1 hour at 4 °C. The final concentration of atelocollagen was 0.05%. Nine weeks after tumor injection, individual mice (from cohorts containing three animals) were injected with 200 μl of atelocollagen containing 50 μg of miR-16 complexed with atelocollagen, or NC miRNA/atelocollagen by intravenous tail-vein injection.

Analysis of miR-16/atelocollagen treatment for bone-metastatic prostate cancer. Mice were inoculated with PC-3M-luc cells into the left cardiac ventricle on day zero as described previously.[13] The miR-16 and NC miRNA (50 μg) with 0.05% atelocollagen in a 200 μl volume were injected into the mouse tail vein on days 4, 7, and 10 postinoculation. Each experimental condition included six animals per group. At the end of the experiment on day 28, to confirm the presence of neoplastic cells, selected tissues were excised from the mice at necropsy. Tissues were fixed in 4% formaldehyde-phosphate-buffered saline(−), embedded in paraffin, cut into 5-μm sections, and stained with hematoxylin and eosin.

Clinical samples. Human prostate tissue samples derived from resected prostates from treatment-naive men with an average age of 65 (range of 52–76) diagnosed with nonmetastatic T2 or T3 prostate adenocarcinoma who gave informed consent. Gleason scores for all patients were 8 or 9. The tissues from patients were formalin-fixed, paraffin-embedded, sectioned, hematoxylin and eosin stained, and subjected to microscopic analysis. Three adjacent sections comprising 60–90% (74% average) cancerous tissue were selected as cancer samples from each patient. Three adjacent sections lacking evidence of cancer cells were selected as normal adjacent

samples. RNA from the tissues were prepared using the RecoverAll Total RNA Isolation Kit (Ambion). The isolated RNA was subjected to qRT-PCR for miR-16 as described above.

MiR-16 functional pathway analysis. For preparation of RNA samples, PC-3M-luc cells were reverse transfected in quadruplicate by complexing miR-16 and NC miRNA and NeoFX transfection reagent (Ambion). The final concentration of miRNA was 30 nmol/l. Cells were harvested at 72 hours post-transfection. One microgram of total RNA per sample was used to prepare biotin-labeled cRNA using a MessageAmp II-based protocol (Ambion) and one round of amplification. Labeled cRNA was hybridized, washed, and scanned using Illumina's recommended protocols. Illumina BeadScan software was used to produce .idat, .xml, and .tif files for each array on a slide. Raw data were extracted using Illumina BeadStudio software, v 3.0 (Illumina, San Diego, CA). Following quality assessment, data from the replicate beads on each array were summarized into average intensity values and variances. The background subtracted data were used to compare the relative expression of mRNAs in cells transfected with miR-16, NC miRNA, and transfection agent only. analysis of variance was used to judge the significance of the variation observed between the various treatment groups. In total, 285 mRNAs exceeded the thresholds used to identify differentially expressed genes (log ratio greater than 0.5 or less than −0.5 for the average signal between miR-16 and NC miRNA or transfection agent only treatments and P values <0.001 for the 72 hour time-point).

Statistical analysis. The results are given as mean ± SD Statistical analysis was conducted using the analysis of variance with the Bonferroni correction for multiple comparisons. A P value of ≤0.05 was considered to indicate a significant difference.

SUPPLEMENTARY MATERIAL

Figure S1. The scheme of dual luciferase assay for monitoring of systemic miR-16 delivery.

Figure S2. Overview of experimental protocol for inhibition of metastatic tumor growth in bone tissues by the atelocollagen-mediated miRNA treatment.

Figure S3. KEGG cell cycle diagram.

Table S1. Data of the mRNA array for comparison of miR-16 and NC miR transfected PC-3M-luc cells.

ACKNOWLEDGMENTS

We thank Ayako Inoue, Ayano Matsumoto, and Maho Kodama for their excellent technical work. We also thank Shunji Nagahara of Formulation Research Laboratories, Technology Research and Development Center, Dainippon Sumitomo Pharma Co., Ltd. for technological support and Koken Co., Ltd. for providing atelocollagen. This work was supported in part by a Grant-in-Aid for the Third-Term Comprehensive 10-Year Strategy for Cancer Control, a Grant-in-Aid for Scientific Research on Priority Areas Cancer from the Ministry of Education, Culture, Sports, Science and Technology, and the Program for Promotion of Fundamental Studies in Health Sciences of the National Institute of Biomedical Innovation (NiBio), and a Takeda Science Foundation.

REFERENCES

1. Calin, GA, Sevignani, C, Dumitru, CD, Hyslop, T, Noch, E, Yendamuri, S *et al.* (2004). Human microRNA genes are frequently located at fragile sites and genomic regions involved in cancers. *Proc Natl Acad Sci USA* **101**: 2999–3004.
2. Calin, GA, Ferracin, M, Cimmino, A, Di Leva, G, Shimizu, M, Wojcik, SE *et al.* (2005). A microRNA signature associated with prognosis and progression in chronic lymphocytic leukemia. *N Engl J Med* **353**: 1793–1801.
3. Calin, GA and Croce, CM (2006). MicroRNA-cancer connection: the beginning of a new tale. *Cancer Res* **66**: 7390–7394.
4. Lu, J, Getz, G, Miska, EA, Alvarez-Saavedra, E, Lamb, J, Peck, D *et al.* (2005). MicroRNA expression profiles classify human cancers. *Nature* **435**: 834–838.
5. Volinia, S, Calin, GA, Liu, CG, Ambs, S, Cimmino, A, Petrocca, F *et al.* (2006). A microRNA expression signature of human solid tumors defines cancer gene targets. *Proc Natl Acad Sci USA* **103**: 2257–2261.
6. Mattie, MD, Benz, CC, Bowers, J, Sensinger, K, Wong, L, Scott, GK *et al.* (2006). Optimized high-throughput microRNA expression profiling provides novel biomarker assessment of clinical prostate and breast cancer biopsies. *Mol Cancer* **5**: 24.
7. Porkka, KP, Pfeiffer, MJ, Waltering, KK, Vessella, RL, Tammela, TL and Visakorpi, T (2007). MicroRNA expression profiling in prostate cancer. *Cancer Res* **67**: 6130–6135.
8. Bonci, D, Coppola, V, Musumeci, M, Addario, A, Giuffrida, R, Memeo, L *et al.* (2008). The miR-15a-miR-16-1 cluster controls prostate cancer by targeting multiple oncogenic activities. *Nat Med* **14**: 1271–1277.
9. Bullrich, F and Croce, CM (2001). Molecular biology of chronic lymphocytic leukemia. In: Cheson, B (ed.). *Chronic Lymphoid Leukemia.* Dekker: New York, pp. 9–32.
10. Dong, JT, Boyd, JC and Frierson, HF (2001). Loss of heterozygosity at 13q14 and 13q21 in high grade, high stage prostate cancer. *Prostate* **49**: 166–171.
11. Calin, GA, Dumitru, CD, Shimizu, M, Bichi, R, Zupo, S, Noch, E *et al.* (2002). Frequent deletions and down-regulation of micro-RNA genes miR15 and miR16 at 13q14 in chronic lymphocytic leukemia. *Proc Natl Acad Sci USA* **99**: 15524–15529.
12. Calin, GA and Croce, CM (2006). Genomics of chronic lymphocytic leukemia microRNAs as new players with clinical significance. *Semin Oncol* **33**: 167–173.
13. Takeshita, F, Minakuchi, Y, Nagahara, S, Honma, K, Sasaki, H, Hirai, K *et al.* (2005). Efficient delivery of small interfering RNA to bone-metastatic tumors by using atelocollagen *in vivo*. *Proc Natl Acad Sci USA* **102**: 12177–12182.
14. Yin, Z, Spitz, MR, Babaian, RJ, Strom, SS, Troncoso, P and Kagan, J (1999). Limiting the location of a putative human prostate cancer tumor suppressor gene at chromosome 13q14.3. *Oncogene* **18**: 7576–7583.
15. Arguello, F, Furlanetto, RW, Baggs, RB, Graves, BT, Harwell, SE, Cohen, HJ *et al.* (1992). Incidence and distribution of experimental metastases in mutant mice with defective organ microenvironments (genotypes Sl/Sld and W/Wv). *Cancer Res* **52**: 2304–2309.
16. Jenkins, DE, Yu, SF, Hornig, YS, Purchio, T and Contag, PR (2003). *In vivo* monitoring of tumor relapse and metastasis using bioluminescent PC-3M-luc-C6 cells in murine models of human prostate cancer. *Clin Exp Metastasis* **20**: 745–756.
17. Cimmino, A, Calin, GA, Fabbri, M, Iorio, MV, Ferracin, M, Shimizu, M *et al.* (2005). miR-15 and miR-16 induce apoptosis by targeting BCL2. *Proc Natl Acad Sci USA* **102**: 13944–13949.
18. Johnson, CD, Esquela-Kerscher, A, Stefani, G, Byrom, M, Kelnar, K, Ovcharenko, D *et al.* (2007). The let-7 microRNA represses cell proliferation pathways in human cells. *Cancer Res* **67**: 7713–7722.
19. Kanehisa, M, Araki, M, Goto, S, Hattori, M, Hirakawa, M, Itoh, M *et al.* (2008). KEGG for linking genomes to life and the environment. *Nucleic Acids Res* **36**(Database issue): D480–D484.
20. Kanehisa, M and Goto, S (2000). KEGG: Kyoto Encyclopedia of Genes and Genomes. *Nucleic Acids Res* **28**: 27–30.
21. Kanehisa, M, Goto, S, Hattori, M, Aoki-Kinoshita, KF, Itoh, M, Kawashima, S *et al.* (2006). From genomics to chemical genomics: new developments in KEGG. *Nucleic Acids Res* **34**(Database issue): D354–D357.
22. Dennis, G, Sherman, BT, Hosack, DA, Yang, J, Gao, W, Lane, HC *et al.* (2003). DAVID: Database for Annotation, Visualization, and Integrated Discovery. *Genome Biol* **4**: P3.
23. Lu, W, Takahashi, H, Furusato, M, Maekawa, S, Nakano, M, Meng, C *et al.* (2006). Allelotyping analysis at chromosome 13q of high-grade prostatic intraepithelial neoplasia and clinically insignificant and significant prostate cancers. *Prostate* **66**: 405–412.
24. Chan, JA, Krichevsky, AM and Kosik, KS (2005). MicroRNA-21 is an antiapoptotic factor in human glioblastoma cells. *Cancer Res* **65**: 6029–6033.
25. Cheng, AM, Byrom, MW, Shelton, J and Ford, LP (2005). Antisense inhibition of human miRNAs and indications for an involvement of miRNA in cell growth and apoptosis. *Nucleic Acids Res* **33**: 1290–1297.
26. Johnson, SM, Grosshans, H, Shingara, J, Byrom, M, Jarvis, R, Cheng, A *et al.* (2005). RAS is regulated by the let-7 microRNA family. *Cell* **120**: 635–647.
27. Lim, LP, Lau, NC, Garrett-Engele, P, Grimson, A, Schelter, JM, Castle, J *et al.* (2005). Microarray analysis shows that some microRNAs downregulate large numbers of target mRNAs. *Nature* **433**: 769–773.
28. Lewis, BP, Burge, CB and Bartel, DP (2005). Conserved seed pairing, often flanked by adenosines, indicates that thousands of human genes are microRNA targets. *Cell* **120**: 15–20.
29. Ovcharenko, D, Jarvis, R, Hunicke-Smith, S, Kelnar, K and Brown, D (2005). High-throughput RNAi screening *in vitro*: from cell lines to primary cells. *RNA* **11**: 985–993.
30. Weil, D, Garçon, L, Harper, M, Duménil, D, Dautry, F and Kress, M (2002). Targeting the kinesin Eg5 to monitor siRNA transfection in mammalian cells. *BioTechniques* **33**: 1244–1248.